Interaction Notes
Note 174
March 1974

Analysis of an L-Shaped Wire Over A Conducting Ground Plane Using the Singularity Expansion Method

K.R. Umashankar and D.R. Wilton
University of Mississippi
University, Mississippi

Abstract

In previous reports, a dipole over a ground plane and an L-wire in free space have been analyzed by the singularity expansion method. In this report, an L-wire with one arm parallel to a ground plane is investigated using the singularity expansion method. Natural frequencies, modal current distributions, and coupling coefficients for plane wave excitation are given.

Transient and sinusoidal steady state responses are constructed from the singularity expansion of the current and charge; the time domain convergence of the solution is illustrated.

74-159

I. INTRODUCTION

A parametric study of a L-shaped wire in free space was carried out in [1] using the singularity Expansion Method (SEM) to determine the influence of the location of the bend and the wire radii on the scattering characteristics of the object. In this study, some of the effects of the introduction of a ground plane on the scattering characteristics of the L-wire are considered.

A set of Hallén-type coupled integral equations are given and using the singularity expansion method the complex natural resonant frequencies, modal current and charge distributions, and the corresponding coupling coefficients are given for a particular L-wire structure. A study is made to determine the influence of the distance of the L-wire from the ground plane on the location of the complex natural resonant frequencies. For a step function plane wave incident on the structure the time domain solution for the current and charge are given with the results compared to those obtained by the direct Fourier inversion of frequency domain results.

II. FORMULATION OF THE HALLÉN-TYPE COUPLED INTEGRAL EQUATIONS FOR THE L-WIRE STRUCTURE OVER A PERFECTLY CONDUCTING GROUND PLANE

For an arbitrary incident field, Hallén-type coupled integral equations for the induced current on a perfectly conducting L-wire structure placed over a perfectly conducting ground plane are formulated. The L-wire structure is in the xz-plane, Fig. 1a, with lengths and radii r,h and a_1,a_2 corresponding to the x and z directed elements respectively. The ground plane is located at z = -d in the xy-plane and its effect on the distribution of the current induced on the L-wire is accounted for by applying image theory principles which allows the ground plane to be removed and an image L-wire structure to be placed at a distance z = -2d. The currents i_x and i_z reside on the surfaces of the perfectly conducting wire elements and the corresponding image currents are given by $-i_x$ and i_z respectively on the x and z directed wire elements (see Fig. 1b).

The Hallén-type coupled integral equations can be formulated separately for the L-wire structure and for its image and then combined using the image properties of the currents. This results in simply a modification of the various kernel functions appearing in the coupled integral equations for the L-wire structure in free space [1].

The following are the resultant coupled integral equations of the Hallén-type for the currents induced on the L-wire structure

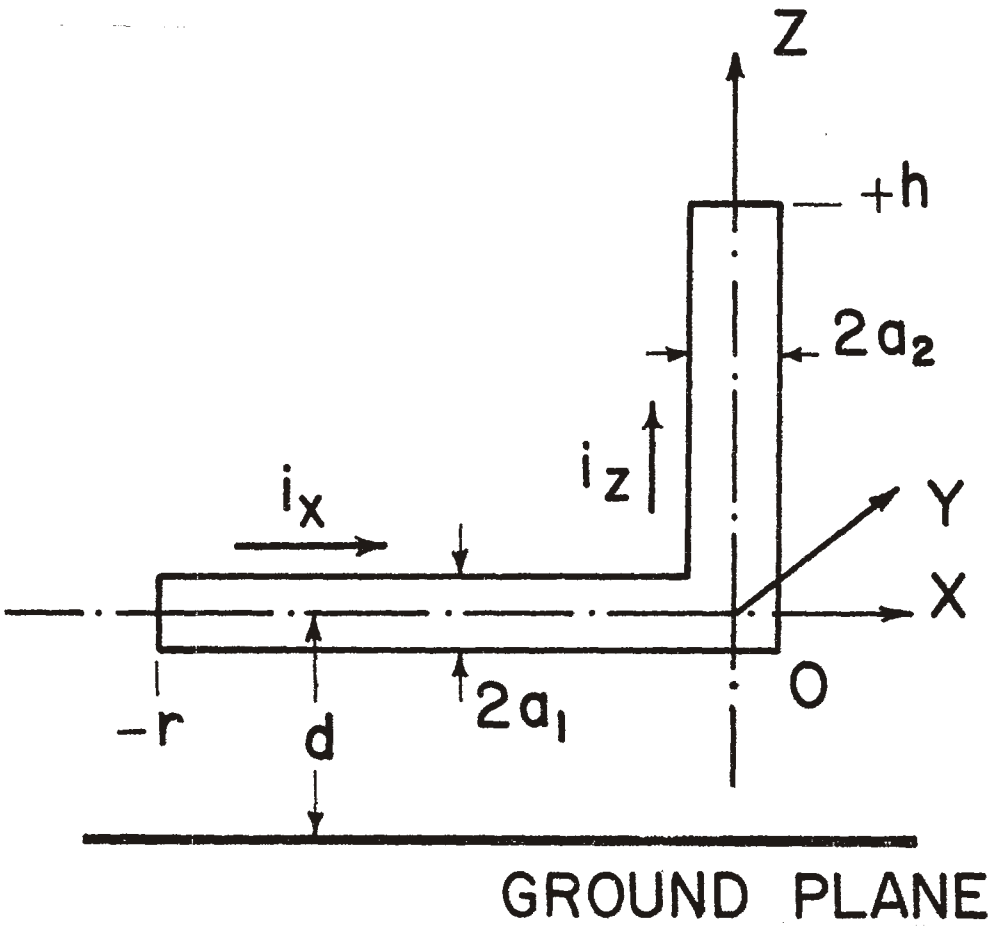

Figure 1a. Geometry of the L-wire structure over a perfectly conducting ground plane.

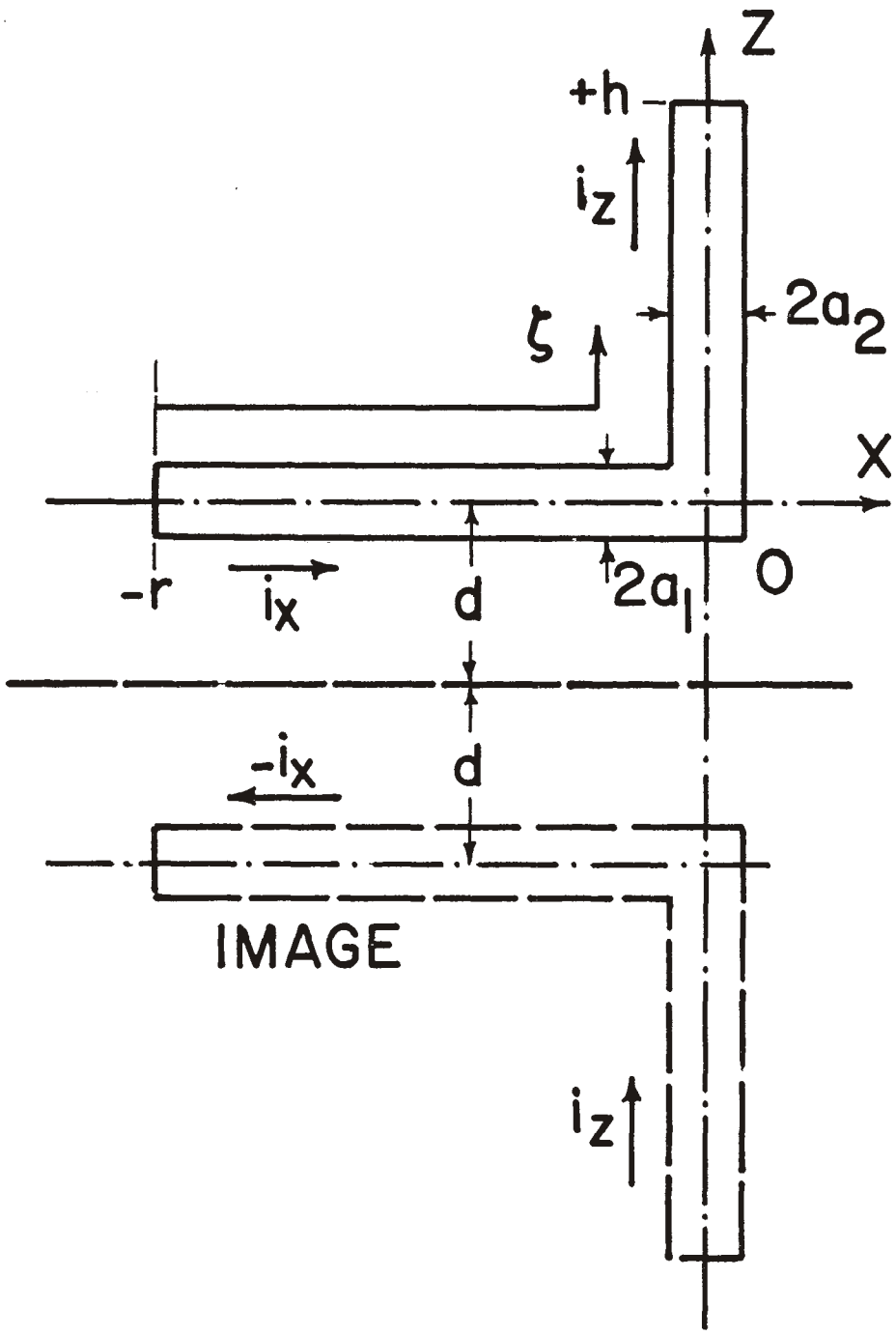

Figure 1b. Ground plane replaced by image.

$$\int_{x'=-r}^{0} i_x(x') \left[K_x(x,x',a_1) - K_x^d(x,x',a_1,-2d) \right] dx'$$

$$+ \int_{z'=0}^{h} i_z(z') \int_{\xi=0}^{x} \left[\frac{\partial}{\partial z} G_z(\xi,a_1,z,z') + \frac{\partial}{\partial z} G_z^d[\xi,a_1,z,-(z'+2d)] \right]_{z=0} \cos k(x-\xi)\, d\xi dz'$$

$$= c_x \cos kx + b \sin kx - j \frac{4\pi}{\eta} \int_{\xi=0}^{x} E_x^i(\xi) \sin k(x-\xi) d\xi, \qquad x\varepsilon(-r,0) \qquad (2.1)$$

$$\int_{x'=-r}^{0} i_x(x') \int_{\zeta=0}^{z} \left[\frac{\partial}{\partial x} G_x(x,x',a_2,\zeta) - \frac{\partial}{\partial x} G_x^d(x,x',a_2,\zeta,-2d) \right]_{x=0} \cos k(z-\zeta)\, d\zeta dx'$$

$$+ \int_{z'=0}^{h} i(z') \left[K_z(a_2,z,z') + K_z^d[a_2,z,-(z'+2d)] \right] dz'$$

$$= c_z \cos kz + b \sin kz - j \frac{4\pi}{\eta} \int_{\zeta=0}^{z} E_z^i(\zeta) \sin k(z-\zeta)\, d\zeta, \qquad z\varepsilon(0,+h) \qquad (2.2)$$

where the various kernel functions are given by:

$$
\left.
\begin{aligned}
K_x(x,x',a_1) &= \frac{e^{-jkR_x}}{R_x}, \quad R_x^2 = a_1^2 + (x-x')^2 \\
K_x^d(x,x',a_1,-2d) &= \frac{e^{-jkR_x^d}}{R_x^d}, \quad R_x^{d^2} = a_1^2 + (x-x')^2 + (2d)^2 \\
G_z(\xi,a_1,z,z') &= \frac{e^{-jkr_z}}{r_z}, \quad r_z^2 = \xi^2 + a_1^2 + (z-z')^2 \\
G_z^d[\xi,a_1,z,-(z'+2d)] &= \frac{e^{-jkr_z^d}}{r_z^d}, \quad r_z^{d^2} = \xi^2 + a_1^2 + (z+z'+2d)^2
\end{aligned}
\right\} \qquad (2.3)
$$

and

$$
\left.
\begin{aligned}
K_z(a_2,z,z') &= \frac{e^{-jkR_z}}{R_z}, \quad R_z^2 = a_2^2 + (z-z')^2 \\
K_z^d[a_2,z,-(z'+2d)] &= \frac{e^{-jkR_z^d}}{R_z^d}, \quad R_z^{d^2} = a_2^2 + (z+z'+2d)^2 \\
G_x(x,x',a_2,\zeta) &= \frac{e^{-jkr_x}}{r_x}, \quad r_x^2 = (x-x')^2 + a_2^2 + \zeta^2 \\
G_x^d(x,x',a_2,\zeta,-2d) &= \frac{e^{-jkr_x^d}}{r_x^d}, \quad r_x^{d^2} = (x-x')^2 + a_2^2 + (\zeta+2d)^2
\end{aligned}
\right\} \qquad (2.4)
$$

located over a perfectly conducting ground plane.

In Equations (2.1) and (2.2), the inside integrals of the double integral terms can be analytically evaluated as in [1] and the resulting expressions are used in the further development of the matrix equation.

We can conveniently write the above integral equations in terms of the Laplace transform variable $s = \sigma + j\omega$ by substituting

$$k = -j\frac{s}{c} \tag{2.5}$$

where k is the wave number of the medium and c is the corresponding velocity of light in the medium.

III. APPLICATION OF THE SINGULARITY EXPANSION METHOD

The complete description of the method of numerical solution to Hallén-type coupled integral equations by using the so-called method of moments [2] and further application of SEM to the matrix equation to determine frequency and time response solutions is given in [1]. First the currents $i_x(x)$ and $i_z(z)$ are represented in terms of piecewise sinusoidal sub-domain expansion functions and the resultant functional equations are "tested" at various match points, Fig. 2, on the structure which results in a partitioned matrix equation for the unknown current coefficients $\overline{I}(s)$,

$$\overline{\overline{Z}}(s)\overline{I}(s) = \overline{V}(s) \tag{3.1}$$

where

$$\overline{\overline{Z}}(s) = \left[\begin{array}{c|c} \overline{\overline{A}} & \overline{\overline{B}} \end{array}\right] \tag{3.2}$$

$$\overline{I}(s) = \left[\begin{array}{c} \overline{J} \\ \hline \overline{C} \end{array}\right] \tag{3.3}$$

$\overline{\overline{A}}$ contains elements of the x and z directed L-wire structure and its image, and $\overline{V}(s)$ is a column vector corresponding to the incident field terms

$$\overline{V}(s) = \left[\begin{array}{c} F_m^x \\ \hline F_\ell^z \end{array}\right] \tag{3.4}$$

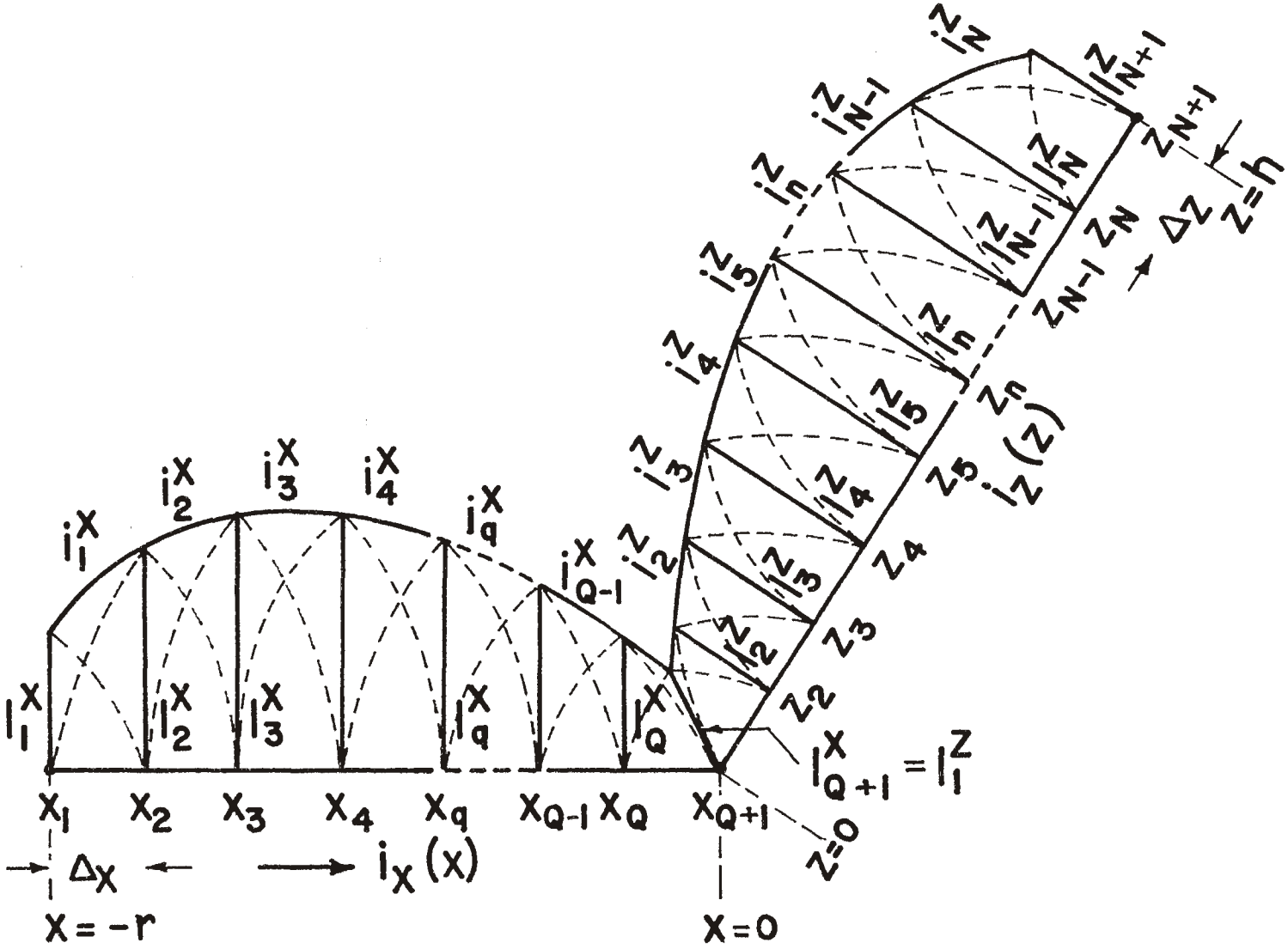

Figure 2. Piecewise sinusoidal basis set and position of match points used in the Hallen-type coupled integral equations.

and F_m^x and F_ℓ^z are given by the integrals

$$F_m^x = -\frac{1}{30}\int_{\xi=0}^{x_m} E_x^i(\xi)\ \sinh\frac{s}{c}(x_m-\xi)d\xi$$

$$F_\ell^z = -\frac{1}{30}\int_{\zeta=0}^{z_\ell} E_z^i(\zeta)\ \sinh\frac{s}{c}(z_\ell-\zeta)d\zeta \qquad (3.5)$$

In the integrals (3.5), $E_x^i(x)$ and $E_z^i(z)$ are the components of the incident field along the x and z directions respectively, evaluated on the scattering structure.

Written in terms of E_θ and E_ϕ polarization components, x and z components of the plane wave incident field are given by

$$E_x^i(x,s) = \left[E_\theta(s)\cos\theta\cos\phi - E_\phi(s)\sin\phi\right]\left[1 - e^{\frac{s}{c}2d\cos\theta}\right] \cdot e^{-\frac{s}{c}\sin\theta\cos\phi\, x} \qquad (3.6)$$

and

$$E_z^i(z,s) = -E_\theta(s)\sin\theta\left[e^{\frac{s}{c}2d\cos\theta}\, e^{\frac{s}{c}\cos\theta\, z} + e^{-\frac{s}{c}\cos\theta\, z}\right] \qquad (3.7)$$

where θ and ϕ are the angles of the incident field with respect to the direction of propagation of the plane wave.

The solution of the matrix Equation (3.1) is given by

$$\overline{I}(s) = \overline{\overline{Z}}^{-1}(s)\ \overline{V}(s) \tag{3.8}$$

According to the singularity expansion method [3], the actual induced current distribution given by the upper partition of the column vector (expression 3.8) can be written as

$$\overline{J}(s) = \sum_i \overline{\overline{Y}}_i^r \frac{\overline{V}(s)}{s-s_i} \tag{3.9}$$

where $s = s_i$ are poles of $\overline{\overline{Z}}^{-1}(s)$ and are the complex natural resonant frequencies of the structure and $\overline{\overline{Y}}_i^r$ denotes the corresponding residue matrix

$$\overline{\overline{Y}}_i^r = \lim_{s \to s_i} (s-s_i)\ \overline{\overline{Z}}^{-1}(s) \tag{3.10}$$

In the previous report [1] methods are described for numerically calculating the natural resonant frequencies and the residue matrix. The mathematical development given in [1] also leads one to rewrite expression (3.9) as

$$\overline{J}(s) = \sum_i \beta_i \overline{J}_i \overline{H}_i^{\dagger} \frac{\overline{V}(s)}{s-s_i} \tag{3.11}$$

where $\bar{J}_i$ is the modal current distribution, $\bar{H}_i$ is the coupling vector corresponding to $s = s_i$ and β_i is a normalization constant. The frequency domain solution corresponding to a time harmonic incident field can be obtained by substituting $s = j\omega$ in the expression (3.11).

To obtain the time domain solution, the Laplace inverse transform of expression (3.11) is found;

$$\bar{i}(t) = L^{-1}\,\bar{J}(s) = \frac{1}{2\pi j}\int_{C_B} \sum_i \frac{\beta_i \bar{J}_i \bar{H}_i^{\dagger}}{s-s_i}\,\bar{V}(s)\,e^{st}\,ds \qquad (3.12)$$

and for the time domain charge distribution,

$$\bar{\rho}(t) = L^{-1}\bar{\rho}(s) = \frac{-1}{2\pi j}\int_{C_B} \sum_i \frac{\beta_i \bar{Q}_i \bar{H}_i^{\dagger}}{s(s-s_i)}\,\bar{V}(s)\,e^{st}\,ds \qquad (3.13)$$

where $\bar{Q}_i = \frac{d\bar{J}_i}{d\zeta}$ is the modal charge distribution at $s = s_i$, and C_B is the Bromwich contour in the complex s-plane.

For a step function plane wave incident, the expression (3.12) becomes

$$\bar{i}(t) = \sum_i \beta_i \bar{J}_i \bar{H}_i^{\dagger}\,\bar{v}_i(t) \qquad (3.14)$$

where

$$\bar{v}_i(t) = [v_{mi}(t)]$$

$$= \left[\frac{1}{2\pi j} \int_{C_B} \frac{V_m(s)e^{st}}{s(s-s_i)}\, ds \right] \tag{3.15}$$

and in the above column vector

$$V_m(s) = \frac{-1}{30} \int_{\xi=0}^{p_m} E_p^i(\xi,s)\, \sinh \frac{s}{c}(p_m-\xi)d\xi \tag{3.16}$$

where

$$p = \begin{cases} x, & m = 1,2, \ldots, Q+1 \\ z, & m = Q+2, \ldots, N+Q+2 \end{cases}$$

and

$$p_m = x_1, x_2, \ldots, x_{Q+1}, z_1, z_2, \ldots, z_{N+1}$$

Hence, substituting (3.16) into (3.15), the element $v_{mi}(t)$ of the column vector (3.15) reduces to the form

$$v_{mi}(t) = \frac{-1}{30} \int_{\xi=0}^{p_m} \left[\frac{1}{2\pi j} \int_{C_B} E_p^i(\xi,s) \left[\frac{1}{s_i(s-s_i)} - \frac{1}{s_i s} \right] \sinh \frac{s}{c}(p_m-\xi)e^{st} ds \right] d\xi \tag{3.17}$$

For E_θ-polarization, the component $E_p^i(\xi,s)$ of the incident electric field is given by the expressions (3.6) and (3.7), and is rewritten below as

$$E_p^i(\xi,s) = A_1 e^{-\frac{s}{c}\gamma_1 \xi} + A_2 e^{-\frac{s}{c}[\gamma_2 \xi - D]} \tag{3.18}$$

where for p = x and m = 1,2,3,...,Q+1

$$A_1 = -A_2 = E_{\theta 0} \cos\theta \cos\phi$$

$$\gamma_1 = \gamma_2 = \sin\theta \cos\phi$$

$$D = 2d \cos\theta$$

and for p = z and m = Q+2,...,N+Q+2

$$A_1 = A_2 = -E_{\theta 0} \sin\theta$$

$$\gamma_1 = -\gamma_2 = \cos\theta$$

$$D = 2d \cos\theta$$

The factor D/c in (3.18) represents the equivalent time delay due to the distance of the L-wire structure over the ground plane. Substituting (3.18) into the expression (3.17), we obtain

$$v_{mi}(t) = \frac{A_1}{60s_i(\gamma_1+1)} \int_{ct+p_m}^{ct-\gamma_1 p_m} u(\tau_1)\left[e^{\frac{s}{c}\tau_1}-1\right]d\tau_1$$

$$- \frac{A_1}{60s_i(\gamma_1-1)} \int_{ct-p_m}^{ct-\gamma_1 p_m} u(\tau_2)\left[e^{\frac{s}{c}\tau_2}-1\right]d\tau_2$$

$$+ \frac{A_2}{60s_i(\gamma_2+1)} \int_{ct+p_m+D}^{ct-\gamma_2 p_m+D} u(\tau_3)\left[e^{\frac{s}{c}\tau_3}-1\right]d\tau_3$$

$$- \frac{A_2}{60s_i(\gamma_2-1)} \int_{ct-p_m+D}^{ct-\gamma_2 p_m+D} u(\tau_4)\left[e^{\frac{s}{c}\tau_4}-1\right]d\tau_4 \qquad (3.19)$$

Because of the presence of the unit step functions in (3.19) due to causality conditions, integration is performed for $\tau_1,\tau_2,\tau_3,\tau_4 > 0$ and whenever at least one of the limits of integration is positive. Hence, the time domain solution is obtained by substituting the expression (3.19) for $v_{mi}(t)$ into (3.14). Similar steps to those of

[1] yield the time domain charge distribution when use is made of Equations (3.13) and (3.17).

IV. NUMERICAL RESULTS

The results of the application of SEM to the L-wire structure over a conducting ground plane are presented in this section for the geometrical parameters $r/L = 0.7$, $a_1/L = a_2/L = 0.001$ and $d/L = 0.5$. In addition, pole trajectories are presented to show the influence of changes in radius and distance above the ground plane. Most of the results found correspond closely with results one would expect on the basis of the results obtained in the previous studies on L-wire [1] and the cylinder above a ground plane [4].

Table 1 gives the location of the complex natural frequencies, which are shown in Figure 3. The figures also serves to identify the indexing convention of the poles. The poles appear to be located in layers parallel to the $j\omega$ - axis, and those poles of the layer closest to the $j\omega$ - axis are slightly perturbed compared to those of the isolated case considered in [1]. The poles located in the remaining layers appear to be due to the interaction between the L-wire and its image. The zigzag shift in the location of successive poles in the layer close to $j\omega$ - axis is due to the location of the bend which closely determines the coupling between the two arms of the L-wire structure [1]. Figures 4 and 5, show the trajectories of the s_{11} and s_{12} poles for a fixed distance over the ground plane when the radius of the L-wire is increased gradually.

ℓ	n	$\frac{\sigma L}{2c}$	$\frac{\omega L}{2c}$
1	1	-0.0748	1.5002
	2	-0.1236	3.1431
	3	-0.2303	4.6759
	4	-0.3142	6.2497
	5	-0.3006	7.8264
	6	-0.3890	9.3958
	7	-0.4033	10.8623
	8	-0.3616	12.4642
	9	-0.4005	14.0902
	10	-0.4790	15.6514
2	1	-1.8661	0.0
	2	-1.5249	3.0182
	3	-1.4977	6.2753
	4	-1.4490	9.4510
3	1	-2.4670	1.0290
	2	-2.1678	3.0309
	3	-1.9680	6.2191
4	1	-3.5845	0.0

Table 1. Natural frequencies of L-wire over ground plane, $r/L = 0.7$, $a_1/L = a_2/L = 0.001$, $d/L = 0.5$.

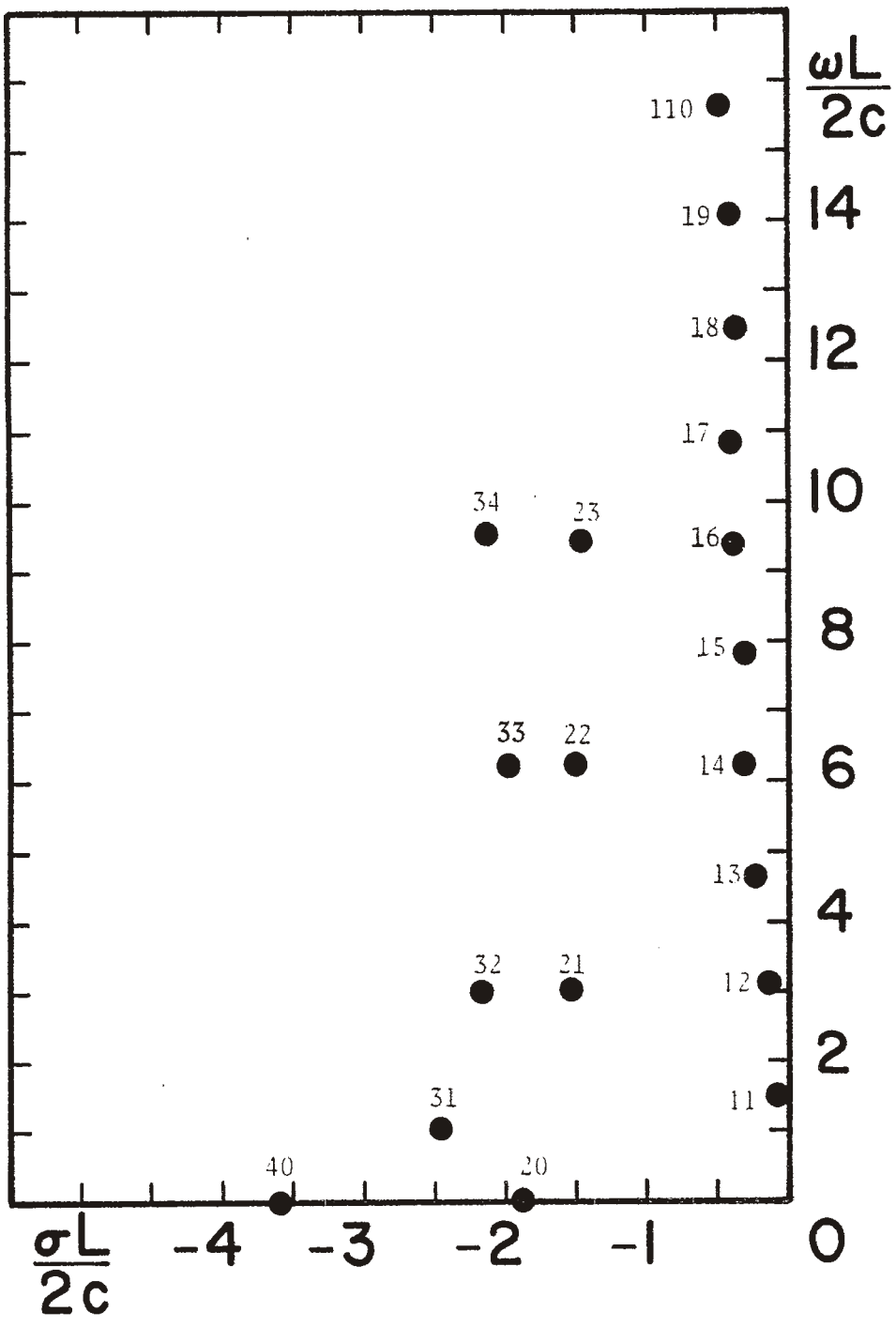

Figure 3. Natural frequencies of L-wire over ground plane, $r/L = 0.7$, $a_1/L = a_2/L = 0.001$, $d/L = 0.5$.

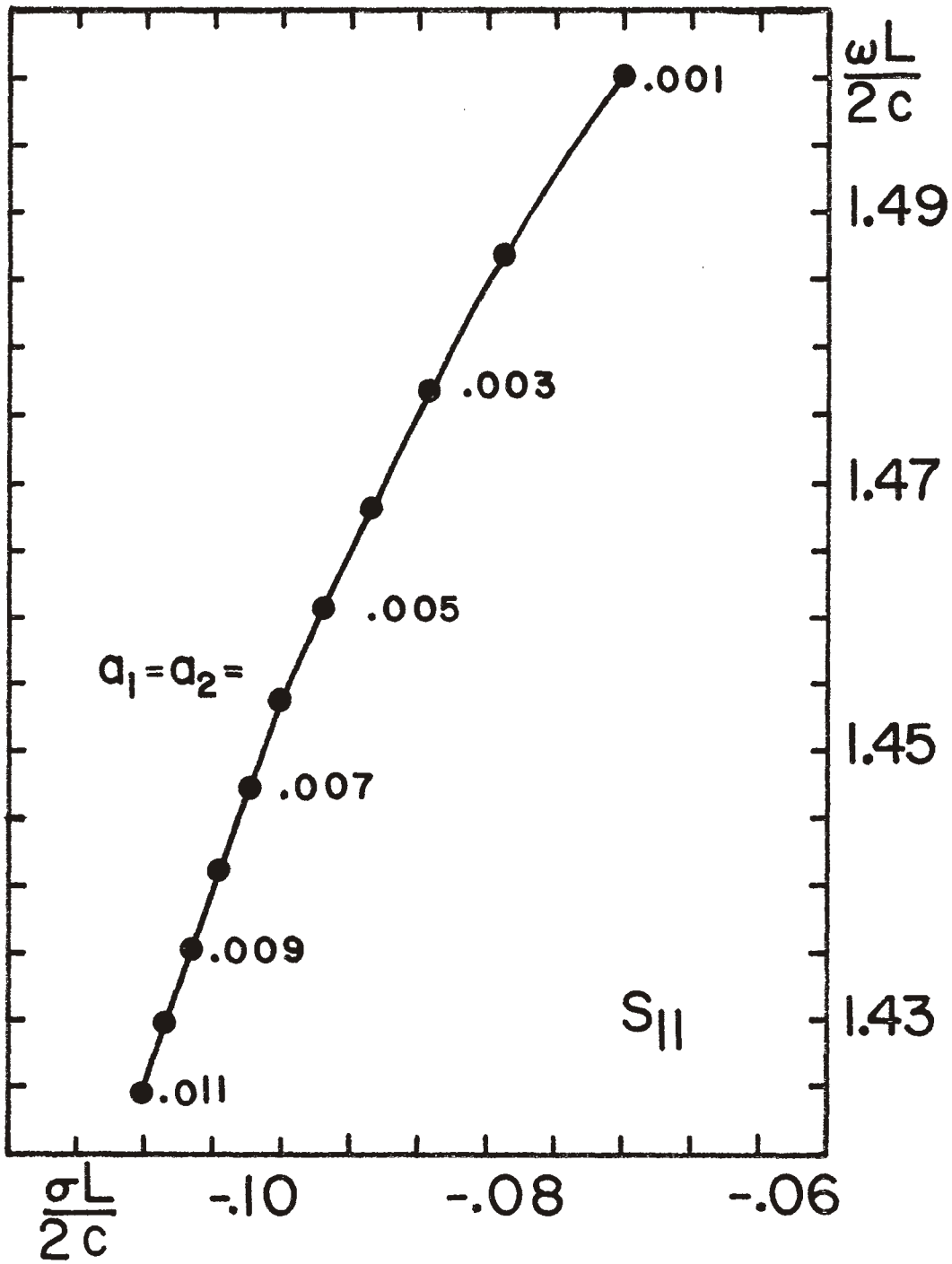

Figure 4. Trajectory of the pole S_{11} as a function of the radius of L-wire, r/L = 0.7, d/L = 0.5.

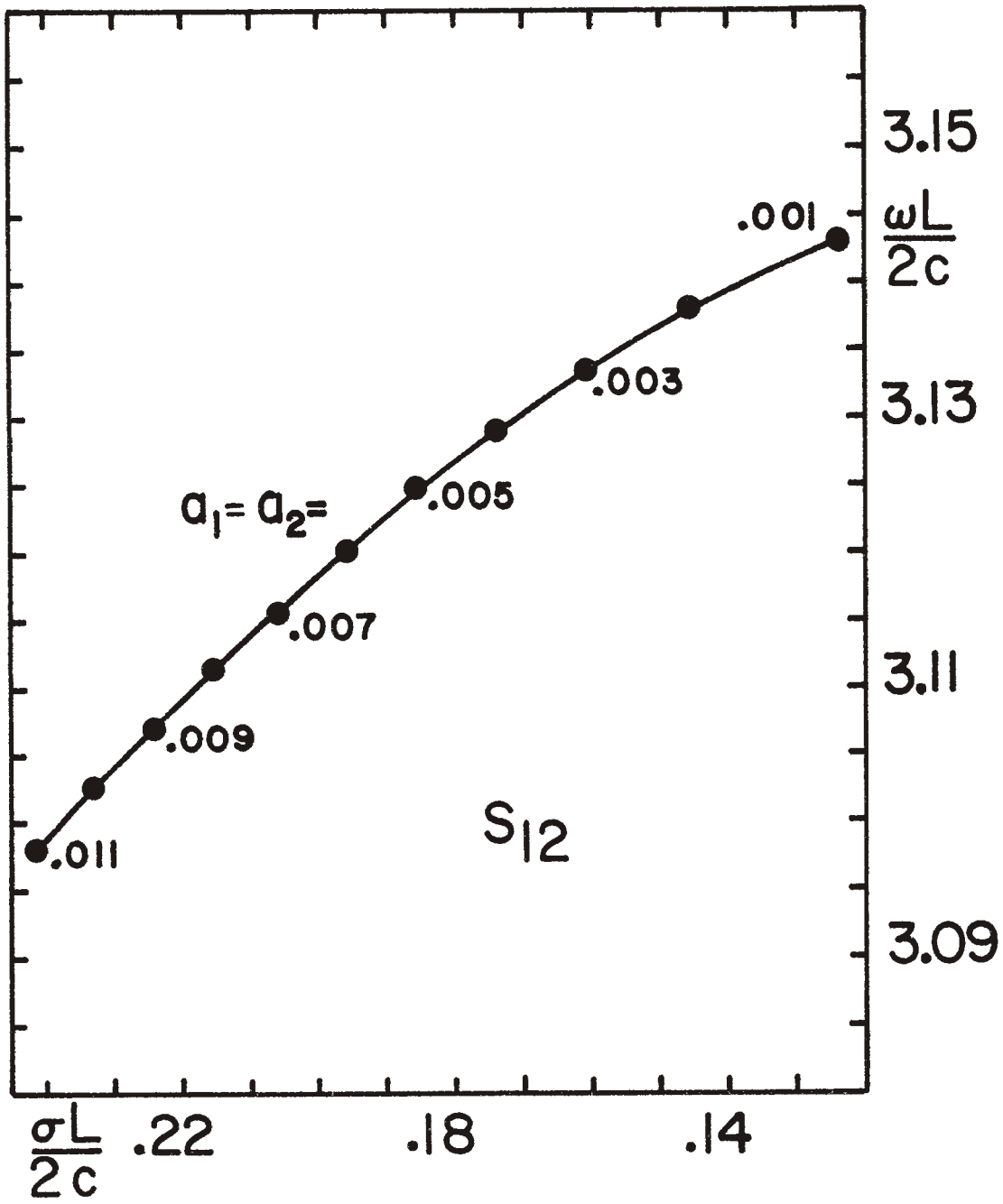

Figure 5. Trajectory of the pole S_{12} as a function of the radius of L-wire, r/L = 0.7, d/L = 0.5.

The trajectories tend to move away from the $j\omega$ - axis, thus introducing more damping into the system as the structure gets thicker. Figure 6 gives the trajectory of s_{11} with the radii of the arms held constant and the distance d over the ground plane gradually increased. A trajectory showing a similarity to those observed for a circular cylinder parallel or perpendicular to a ground plane [4] is also apparent in the present case of the L-wire over the ground plane. The trajectory apparently spirals around the pole location corresponding to the isolated case until another pole from the next layer enters into its path. In Figure 7, the second layer pole trajectories are traced and as the distance to the ground plane is increased, they tend to move towards $s = 0$. Apparently, for thin structures poles of the second layer pass close to and interact with, but ultimately miss the spiral trajectory of the s_{1n} layer as d is increased. However, the closer the secondary layer trajectories come to s_{11}, say, the more perturbed the s_{11} spirals become. In Figure 8, the trajectory of s_{12} is shown as the distance over the ground plane is increased. The trajectories for the second layer poles are shown in Figure 8 and are plotted with an alternative normalization in Figure 9. The normalization to distance above the ground plane in Figure 9 emphasizes the association of these poles with L-wire to its image interactions, as seen by the relative insensitivity of the imaginary part of the (normalized) resonant frequency to changes in d.

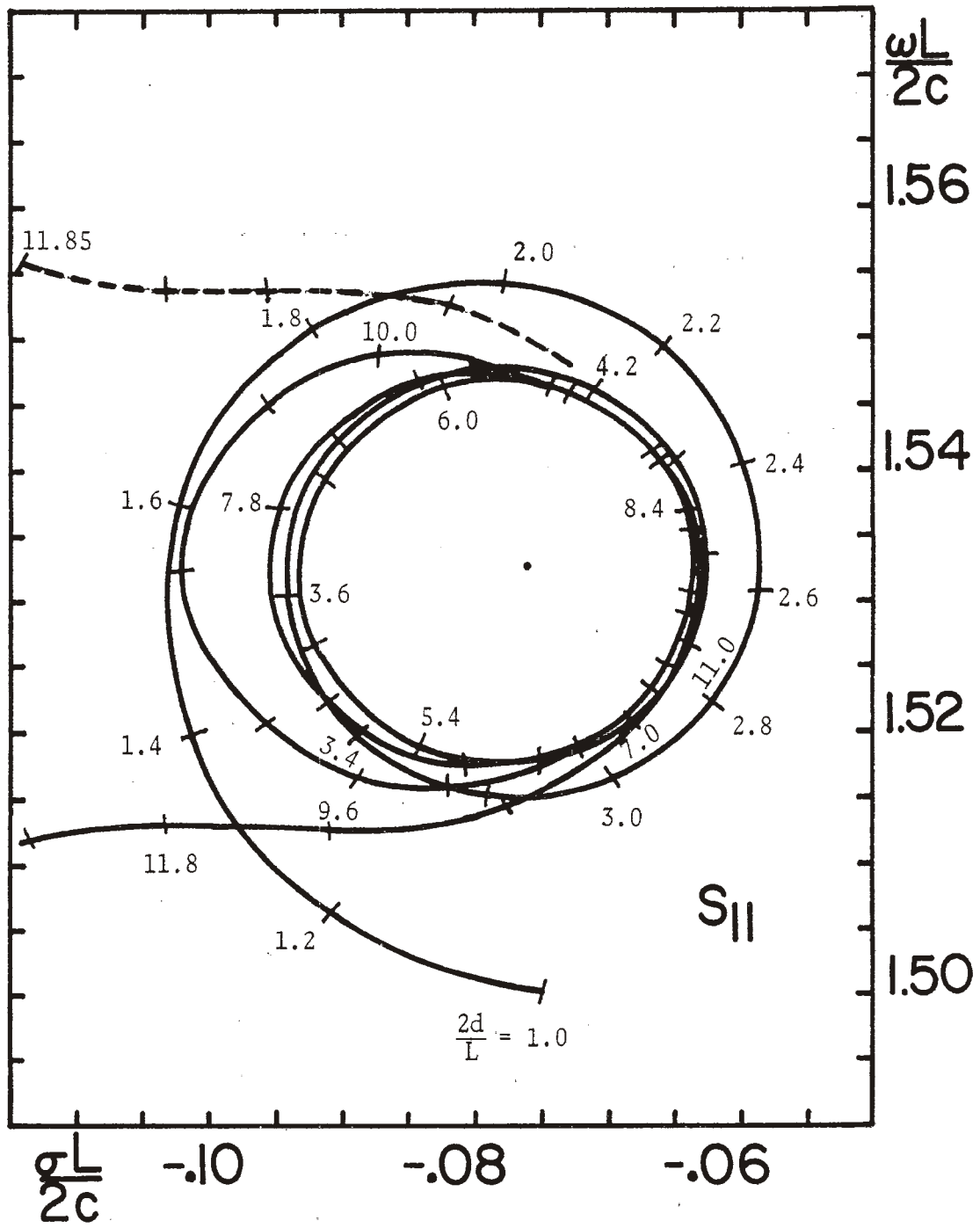

Figure 6. Trajectory of the pole S_{11} as a function of the distance of L-wire from the ground plane, r/L = 0.7, $a_1/L = a_2/L = 0.001$.

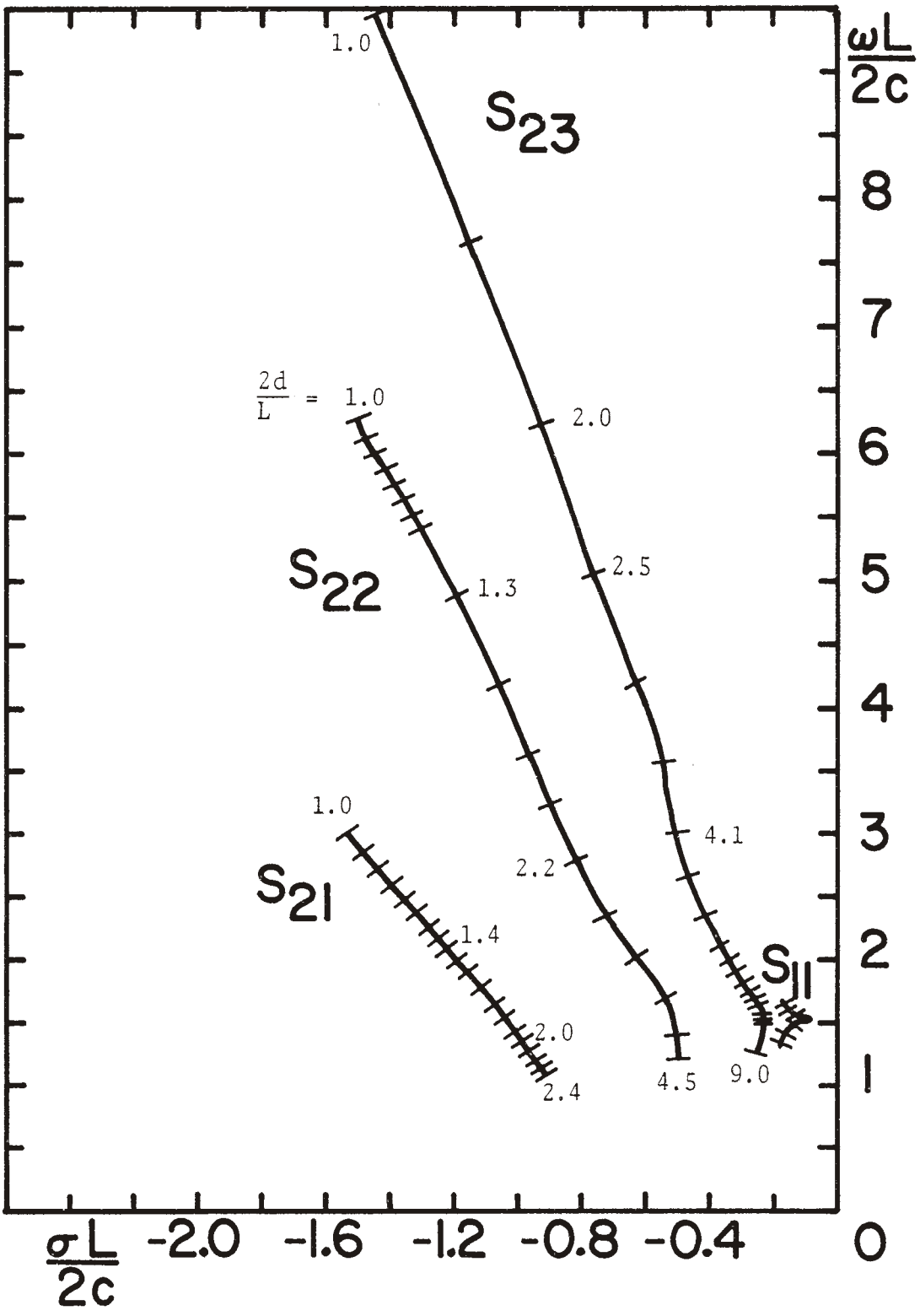

Figure 7. Trajectories of the second layer poles S_{21}, S_{22} and S_{23} as a function of the distance of L-wire from the ground plane, $r/L = 0.7$, $a_1/L = a_2/L = 0.001$.

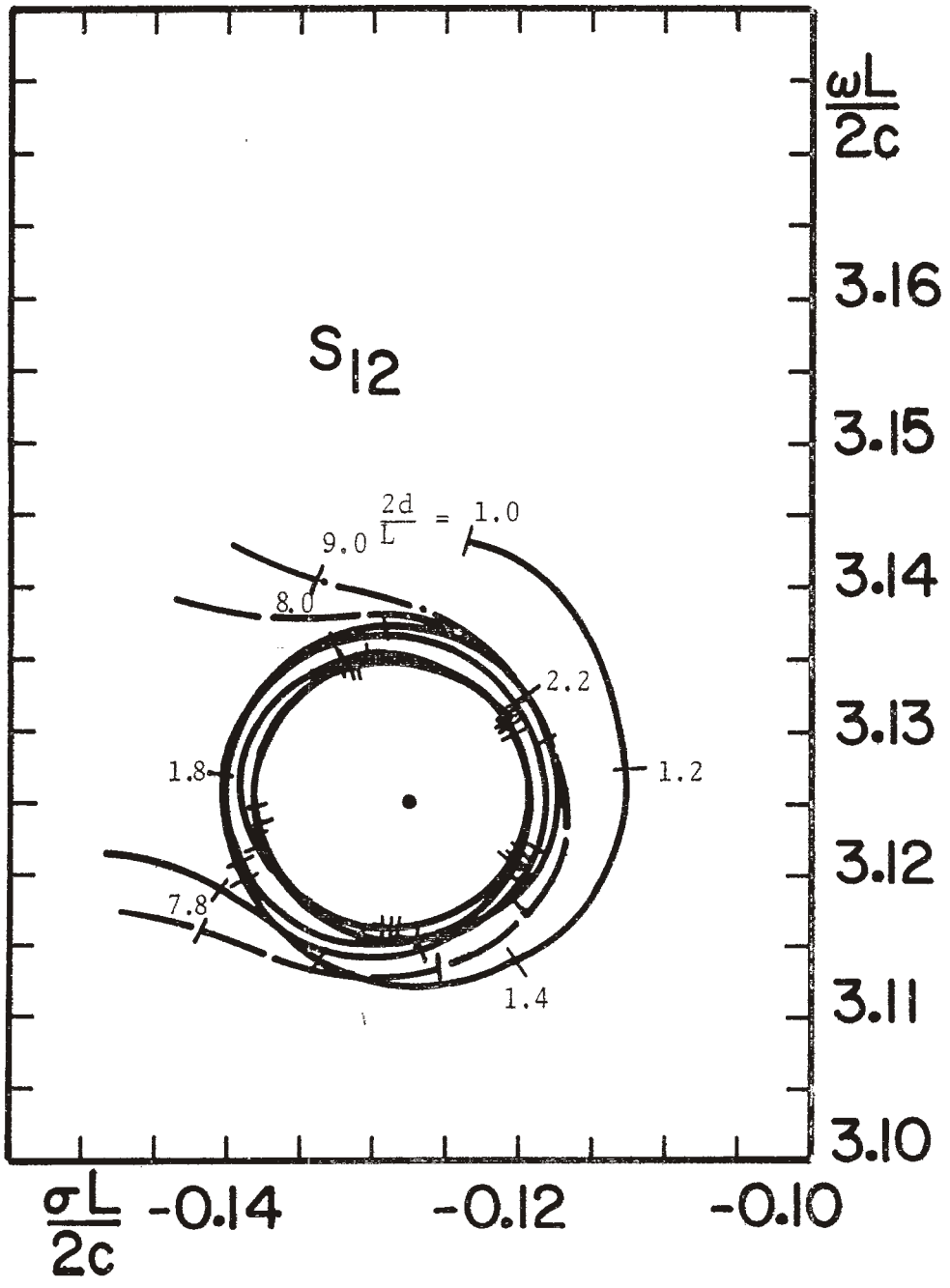

Figure 8. Trajectory of the pole S_{12} as a function of the distance of L-wire from the ground plane, r/L = 0.7, $a_1/L = a_2/L = 0.001$.

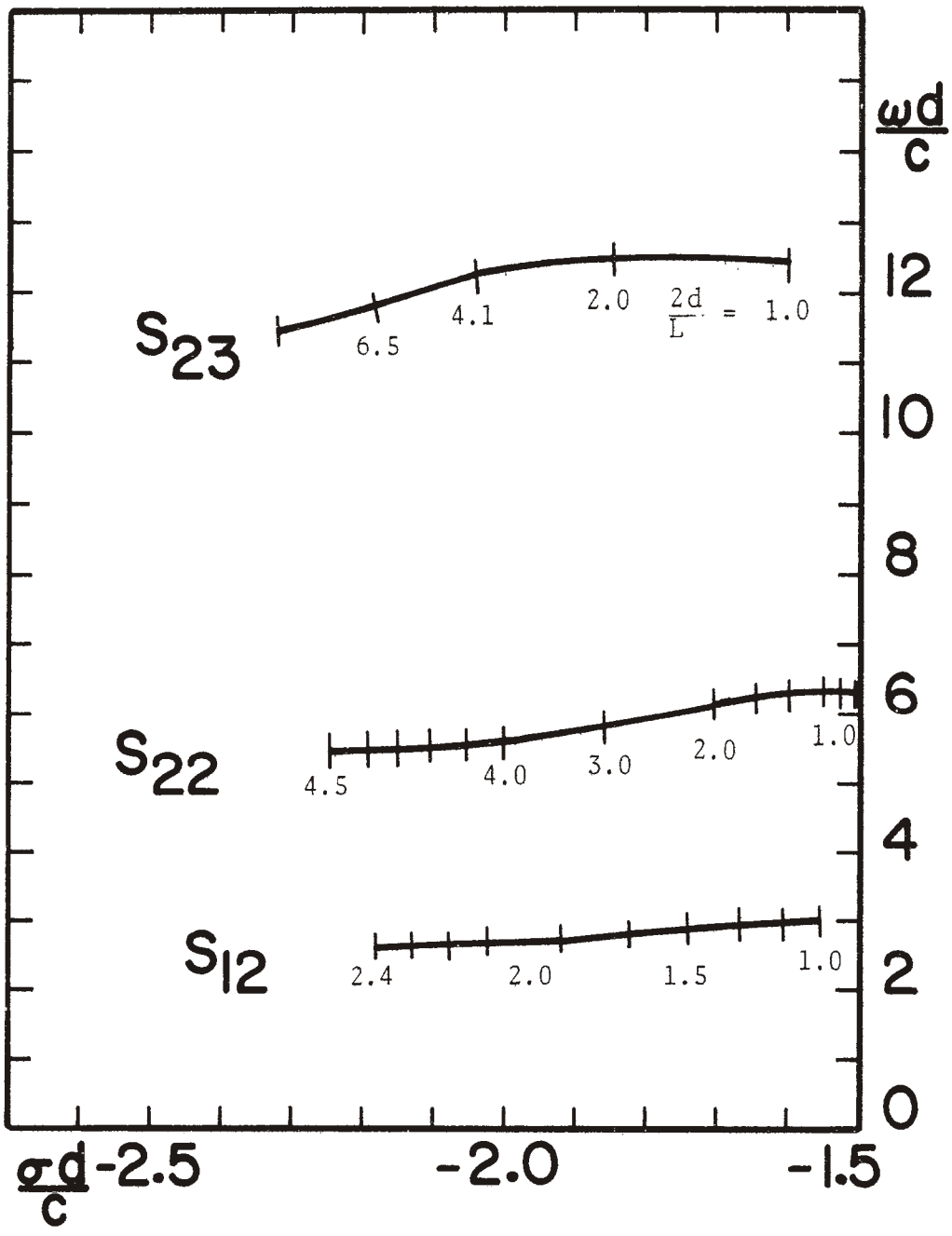

Figure 9. Trajectories of the second layer poles S_{21}, S_{22} and S_{23} as a function of the distance of L-wire from the ground plotted with distance d as the scale factor, $r/L = 0.7$, $a_1/L = a_2/L = 0.001$.

In Figures 10-12 are shown the real and imaginary parts of the modal current distributions corresponding to the first layer poles. Their distribution along the L-wire structure is not only influenced by the location of the bend as was found in [1], but also by the distance of the structure from the ground plane. However, the numerical results show that these influences are relatively minor.

The coupling coefficients $C_{\alpha \ell n}$ and $C_{\beta \ell n}$ corresponding to the first eight poles close to the $j\omega$ - axis are calculated for a delta function plane wave incident which excites the bend at $t = 0$ and are presented in Figures (13-15). Also Figures 16 and 17 show the $C_{\alpha \ell n}$ and $C_{\beta \ell n}$ coupling coefficients of s_{11} and s_{12} poles as the distance over the ground plane is increased. These coupling coefficients are similar to those defined in [1] wherein the incident field is resolved into two linearly independent components one of which excites the horizontal and the other excites the vertical arm, respectively, of the structure. The reflection of the incident field from the ground plane is ignored in the definition of the coupling coefficients since the effect of the reflected wave may be simply treated by superposition of the appropriate plane wave.

The coupling coefficient C_i[3] is given by the expression

$$C_i = \beta_i \overline{H}_i^{\dagger} \; \overline{V}(s_i) \tag{4.1}$$

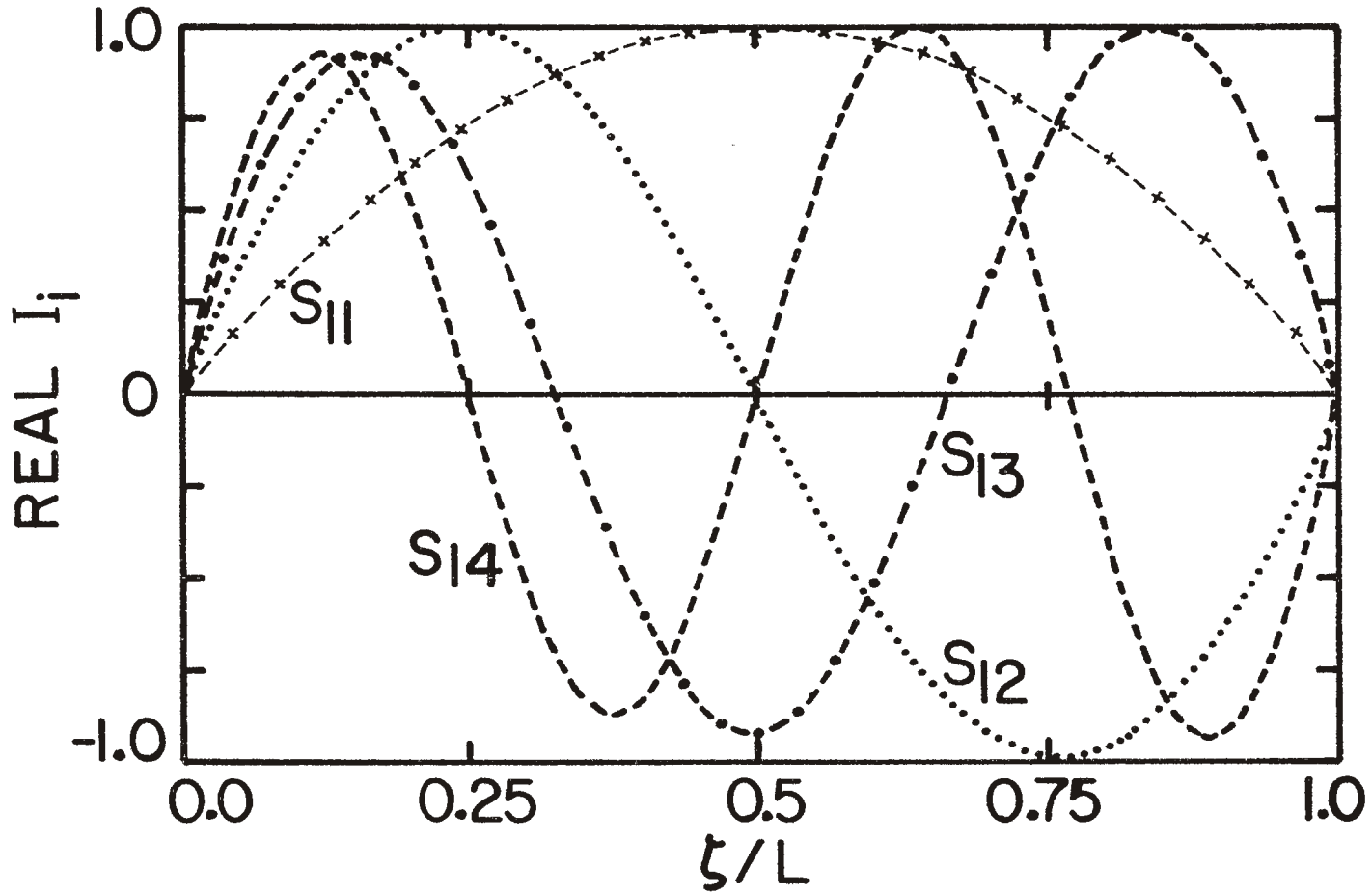

Figure 10a. Real part of the current distribution of the natural modes of an L-wire over a ground plane for resonant frequencies S_{11},S_{12},S_{13} and S_{14}, r/L = 0.7, d/L = 0.5, $a_1/L = a_2/L = 0.001$.

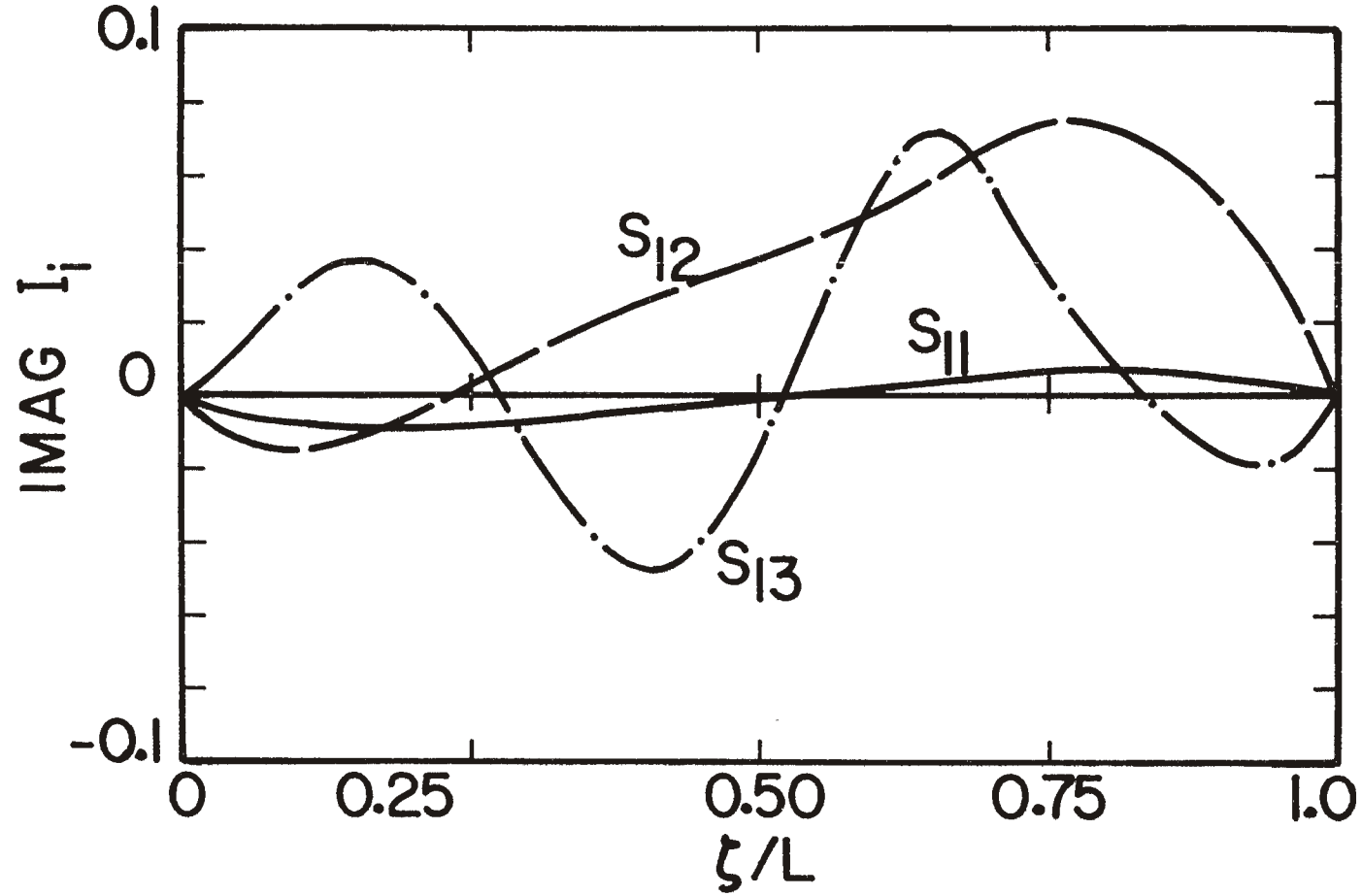

Figure 10b. Imaginary part of the current distribution of the natural modes of an L-wire over a ground plane for resonant frequencies S_{11},S_{12}, and S_{13}, r/L = 0.7, d/L = 0.5, $a_1/L = a_2/L = 0.001$.

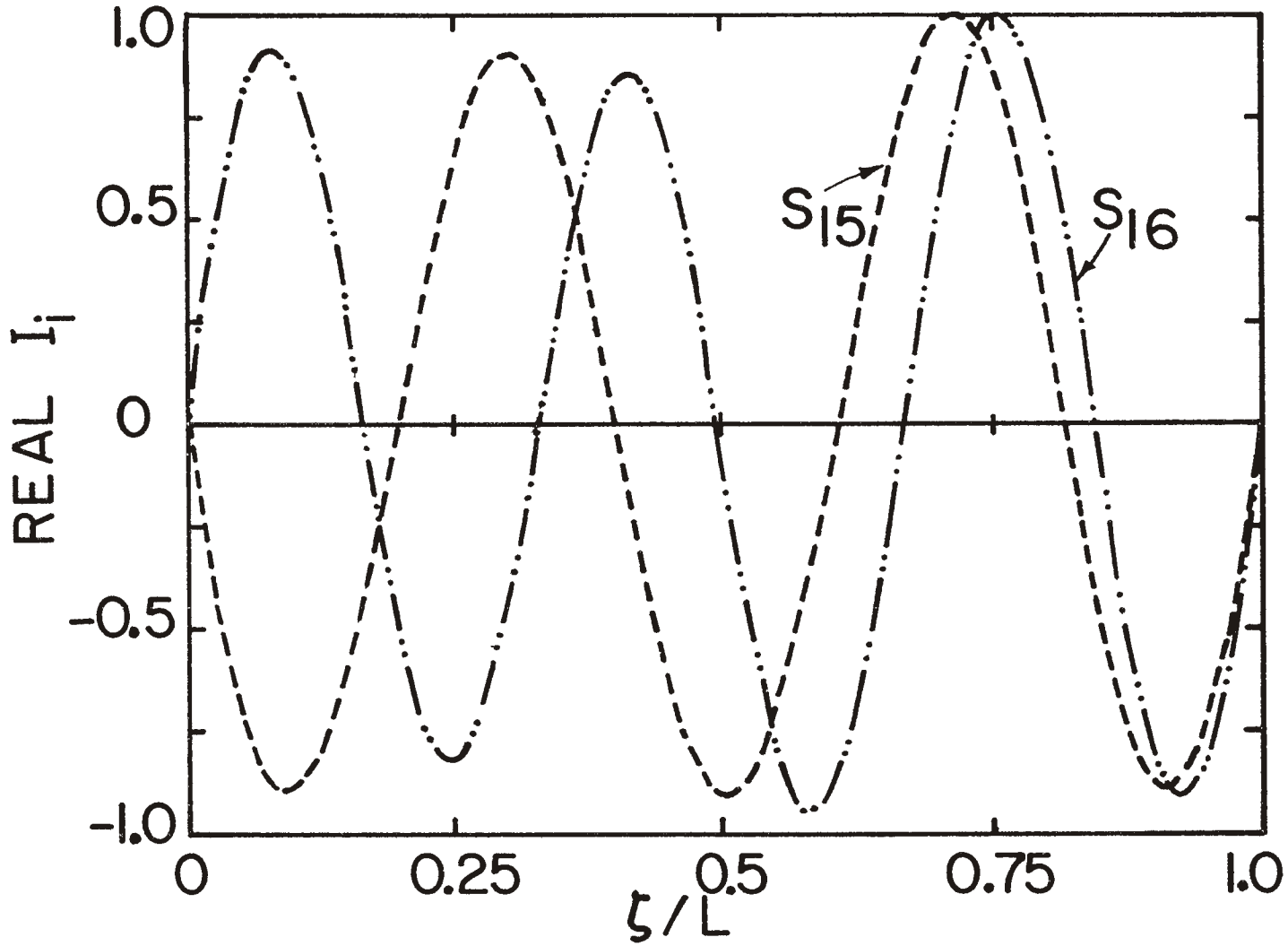

Figure 11a. Real part of the current distribution of the natural modes of an L-wire over a ground plane for resonant frequencies S_{15} and S_{16}, r/L = 0.7, d/L = 0.5, $a_1/L = a_2/L = 0.001$.

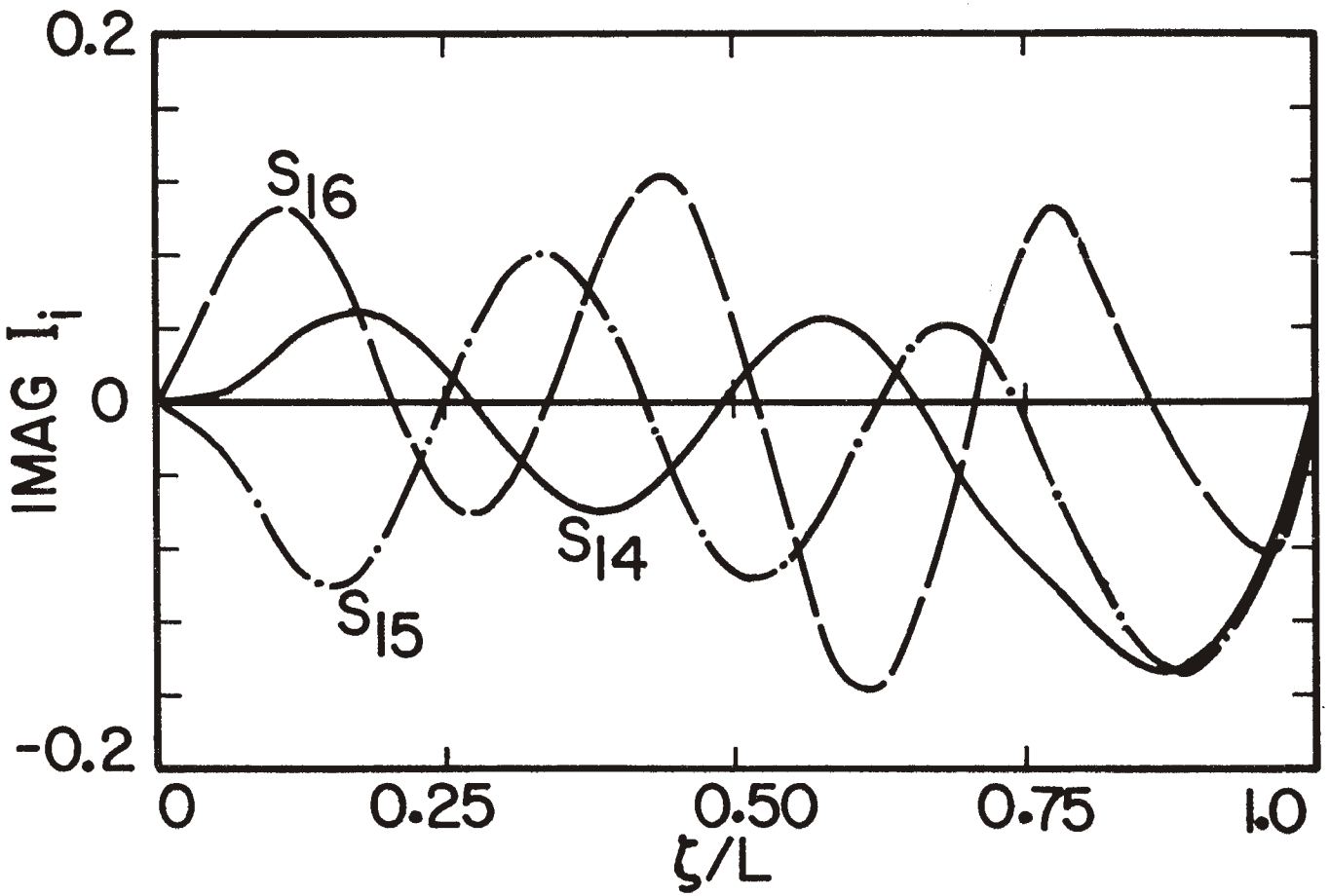

Figure 11b. Imaginary part of the current distribution of the natural modes of an L-wire over a ground plane for resonant frequencies S_{14},S_{15} and S_{16}, r/L = 0.7, d/L = 0.5, $a_1/L = a_2/L = 0.001$.

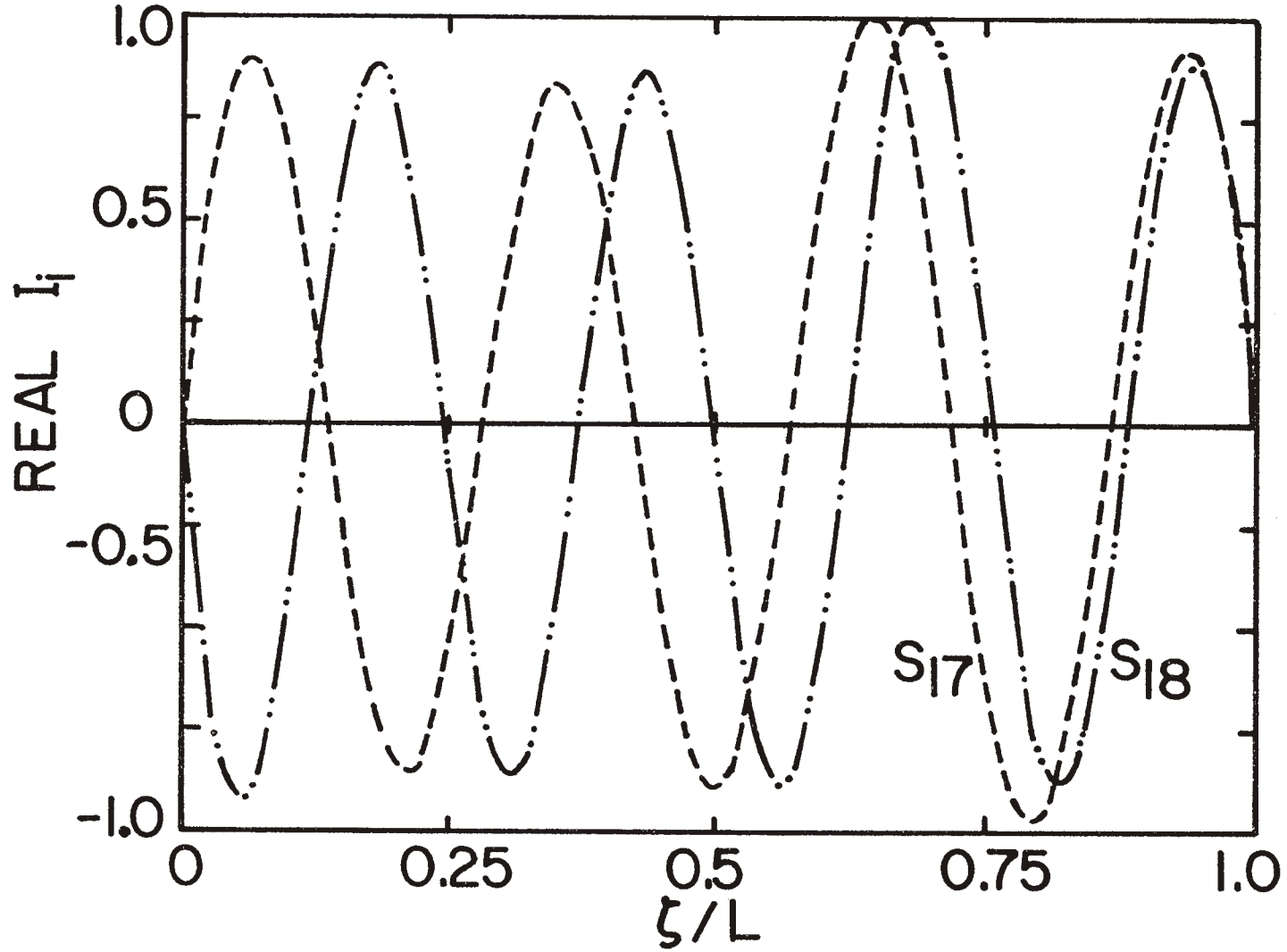

Figure 12a. Real part of the current distribution of the natural modes of an L-wire over a ground plane for resonant frequencies S_{17} and S_{18}, r/L = 0.7, d/L = 0.5, $a_1/L = a_2/L = 0.001$.

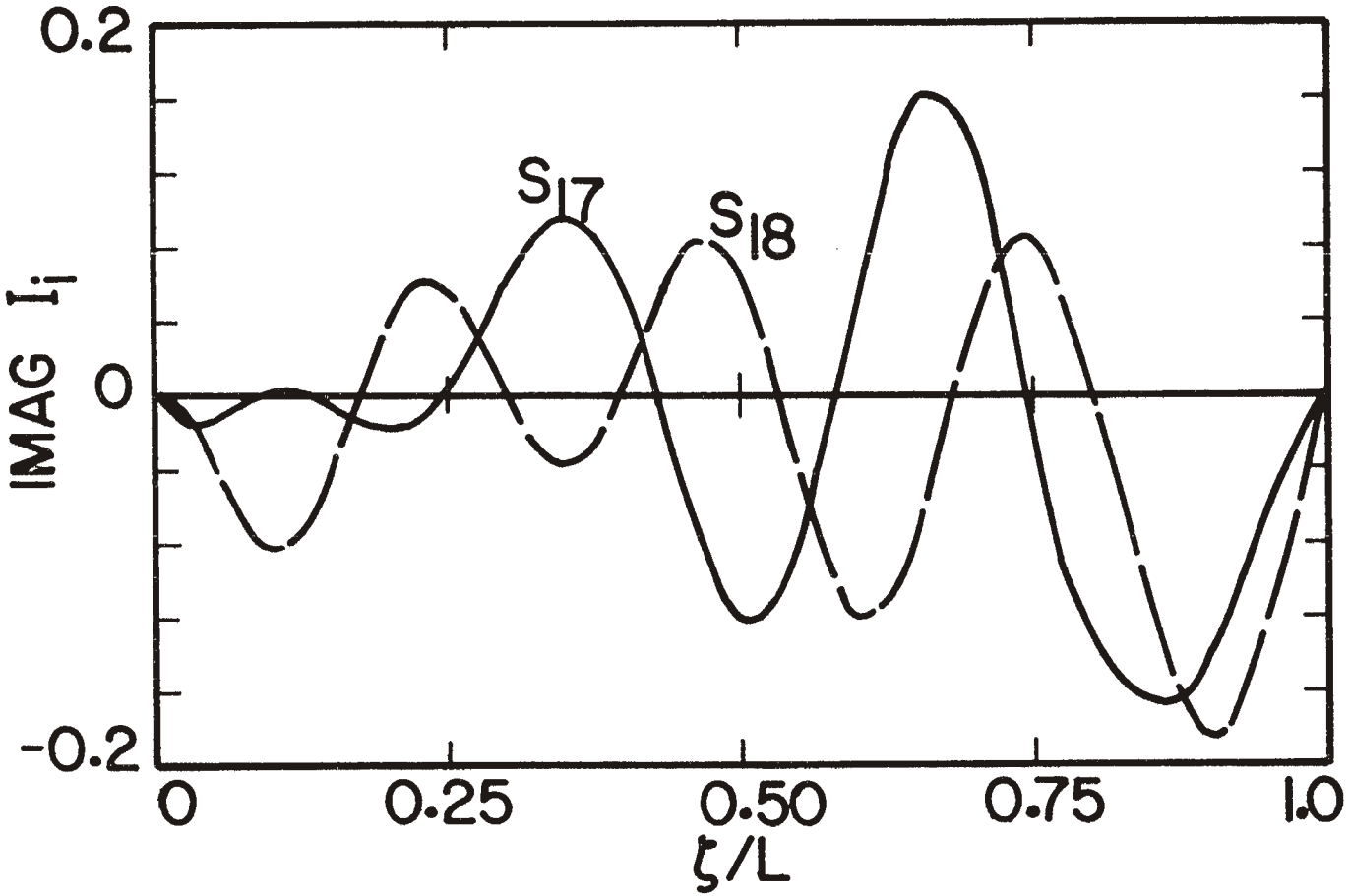

Figure 12b. Imaginary part of the current distribution of the natural modes of an L-wire over a ground plane for resonant frequencies S_{17} and S_{18}, r/L = 0.7, d/L = 0.5, a_1/L = a_2/L = 0.001.

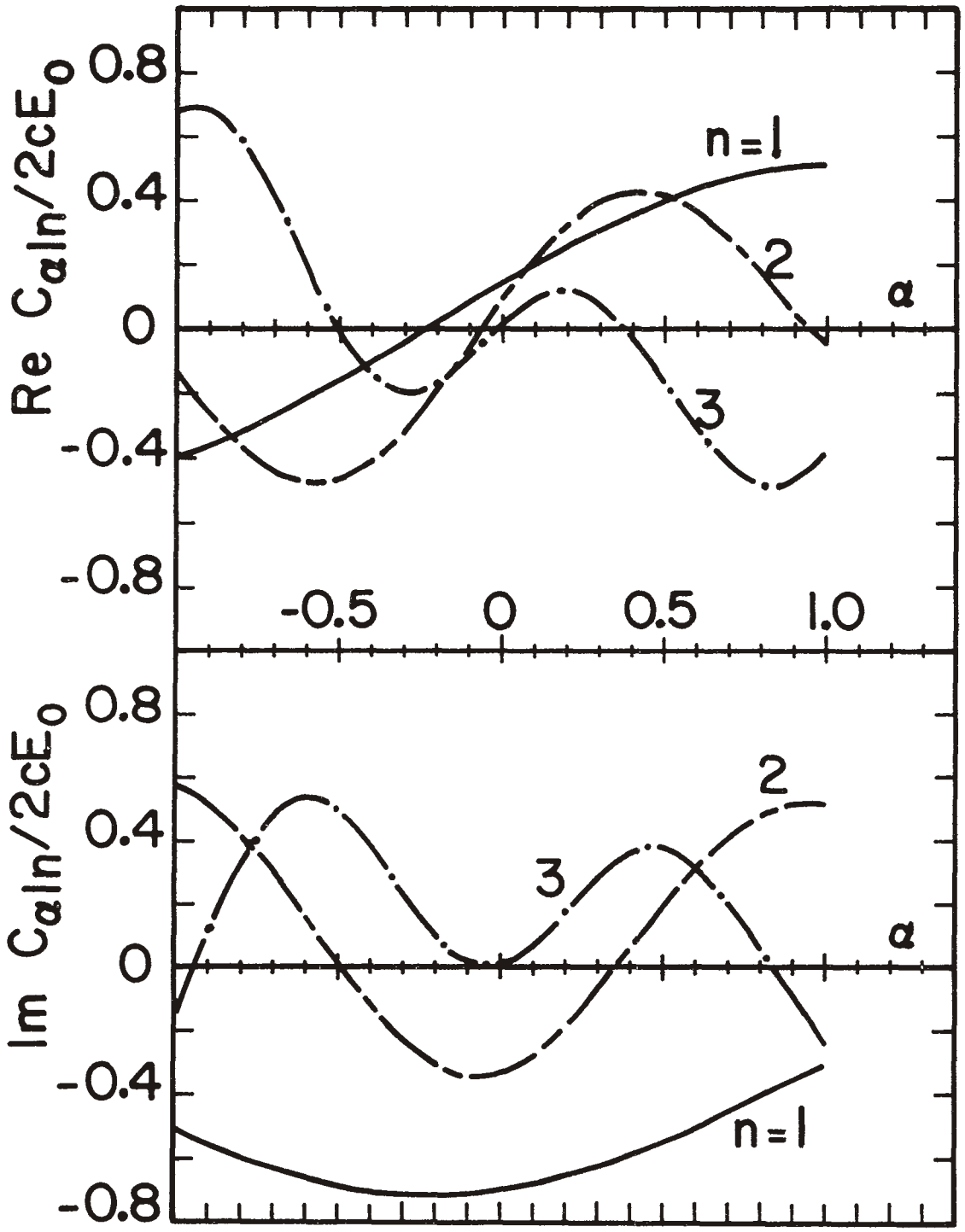

Figure 13a. Coupling coefficient C_α in milliamperes of an L-wire over a ground plane for resonant frequencies S_{11}, S_{12} and S_{13}, r/L = 0.7, d/L = 0.5, $a_1/L = a_2/L = 0.001$.

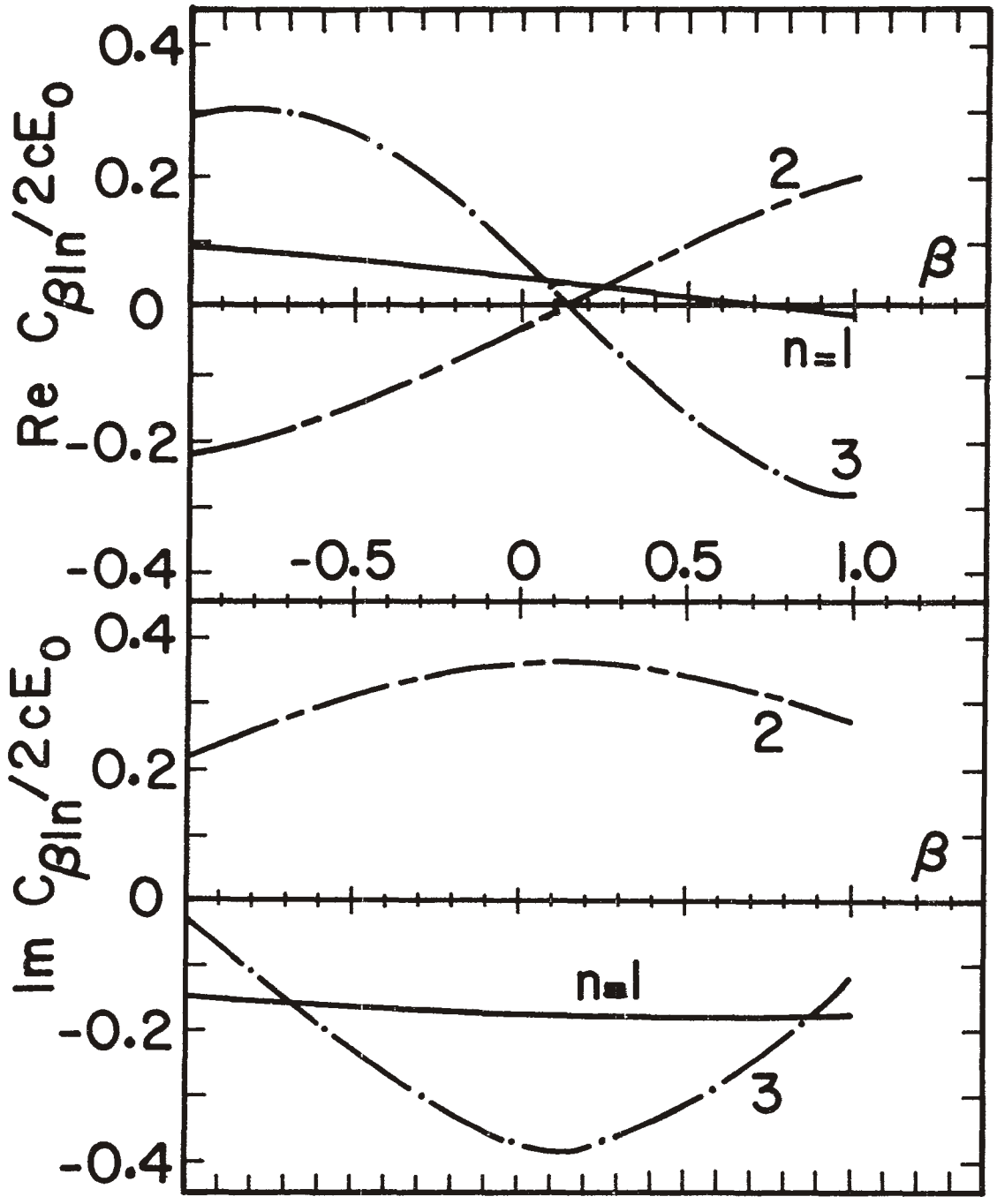

Figure 13b. Coupling coefficient C_β in milliamperes of an L-wire over a ground plane for resonant frequencies S_{11}, S_{12} and S_{13}, r/L = 0.7, d/L = 0.5, $a_1/L = a_2/L = 0.001$.

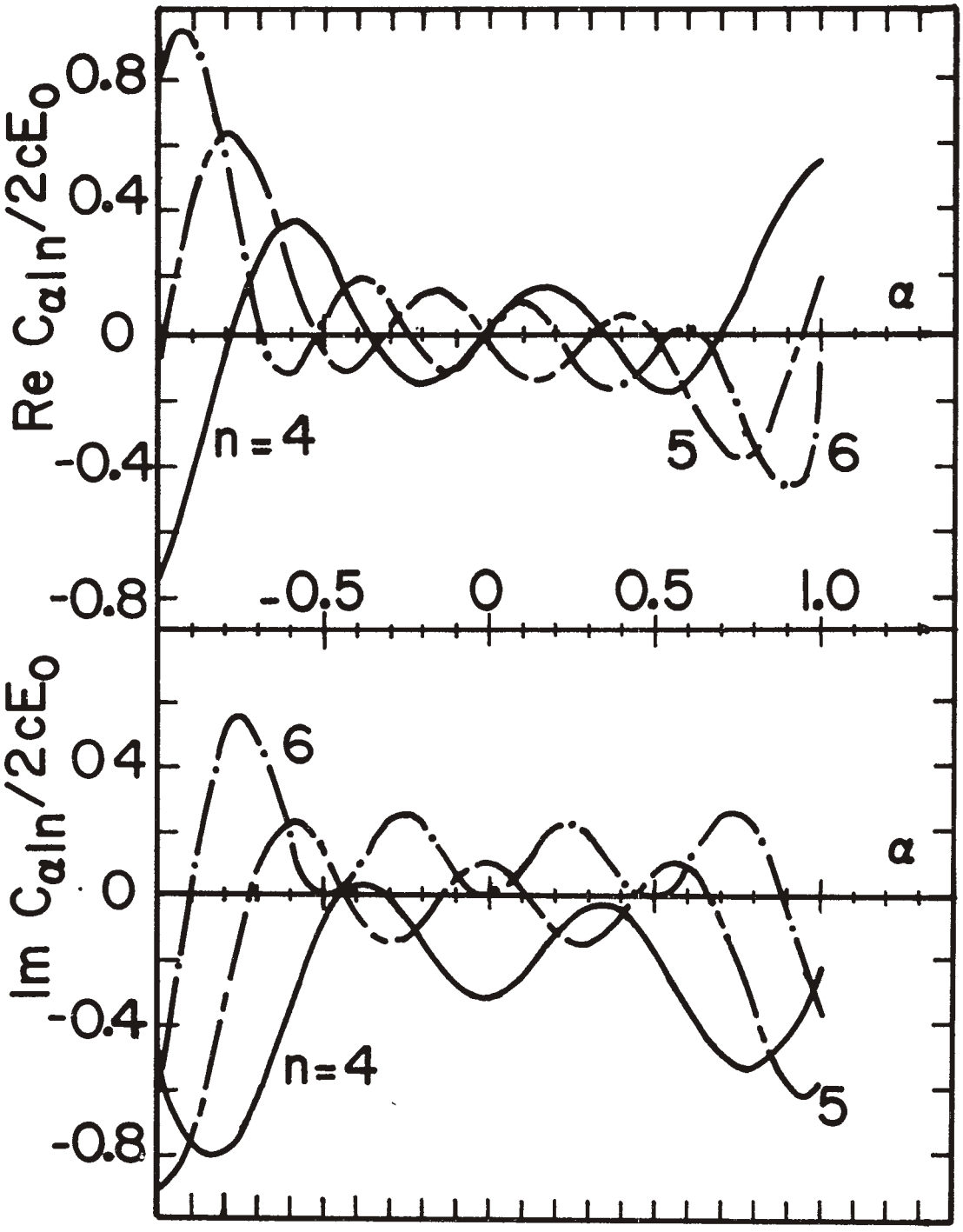

Figure 14a. Coupling coefficient C_α in milliamperes of an L-wire over a ground plane for resonant frequencies S_{14}, S_{15} and S_{16}, r/L = 0.7, d/L = 0.5, $a_1/L = a_2/L = 0.001$.

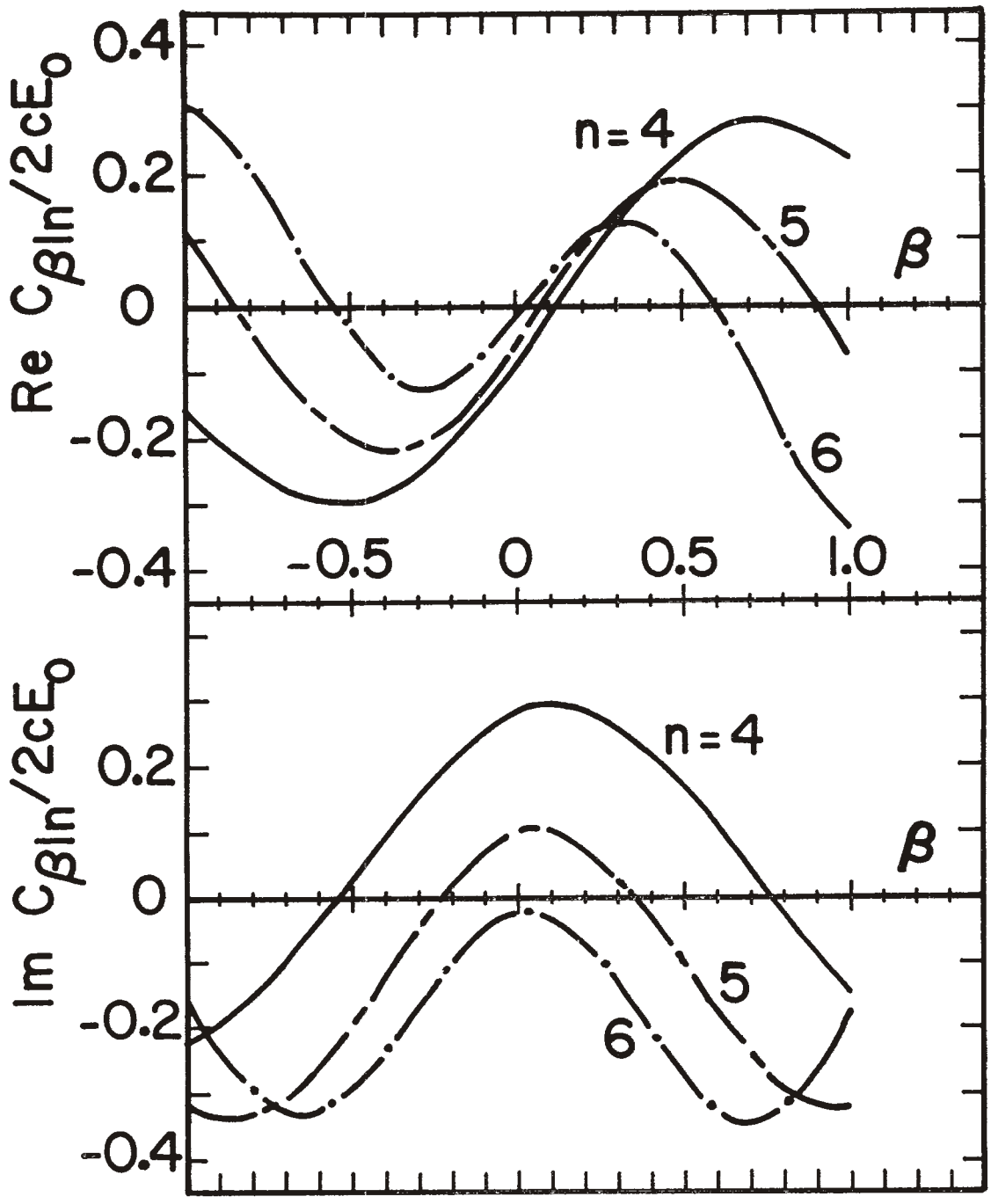

Figure 14b. Coupling coefficient C_β in milliamperes of an L-wire over a ground plane for resonant frequencies S_{14},S_{15} and S_{16}, r/L = 0.7, d/L = 0.5, $a_1/L = a_2/L = 0.001$.

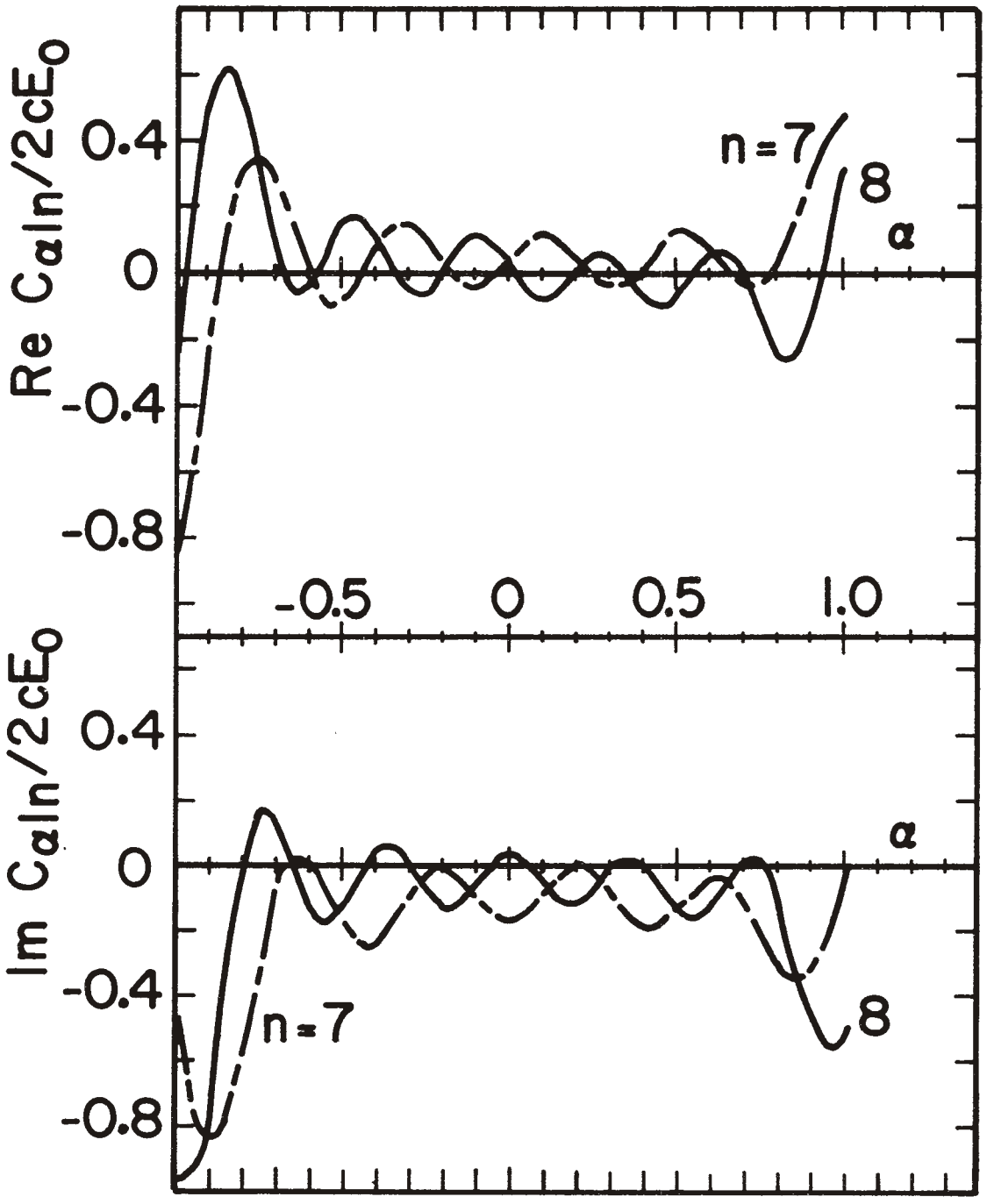

Figure 15a. Coupling coefficient C_α in milliamperes of an L-wire over a ground plane for resonant frequencies S_{17} and S_{18}, r/L = 0.7, d/L = 0.5, $a_1/L = a_2/L = 0.001$.

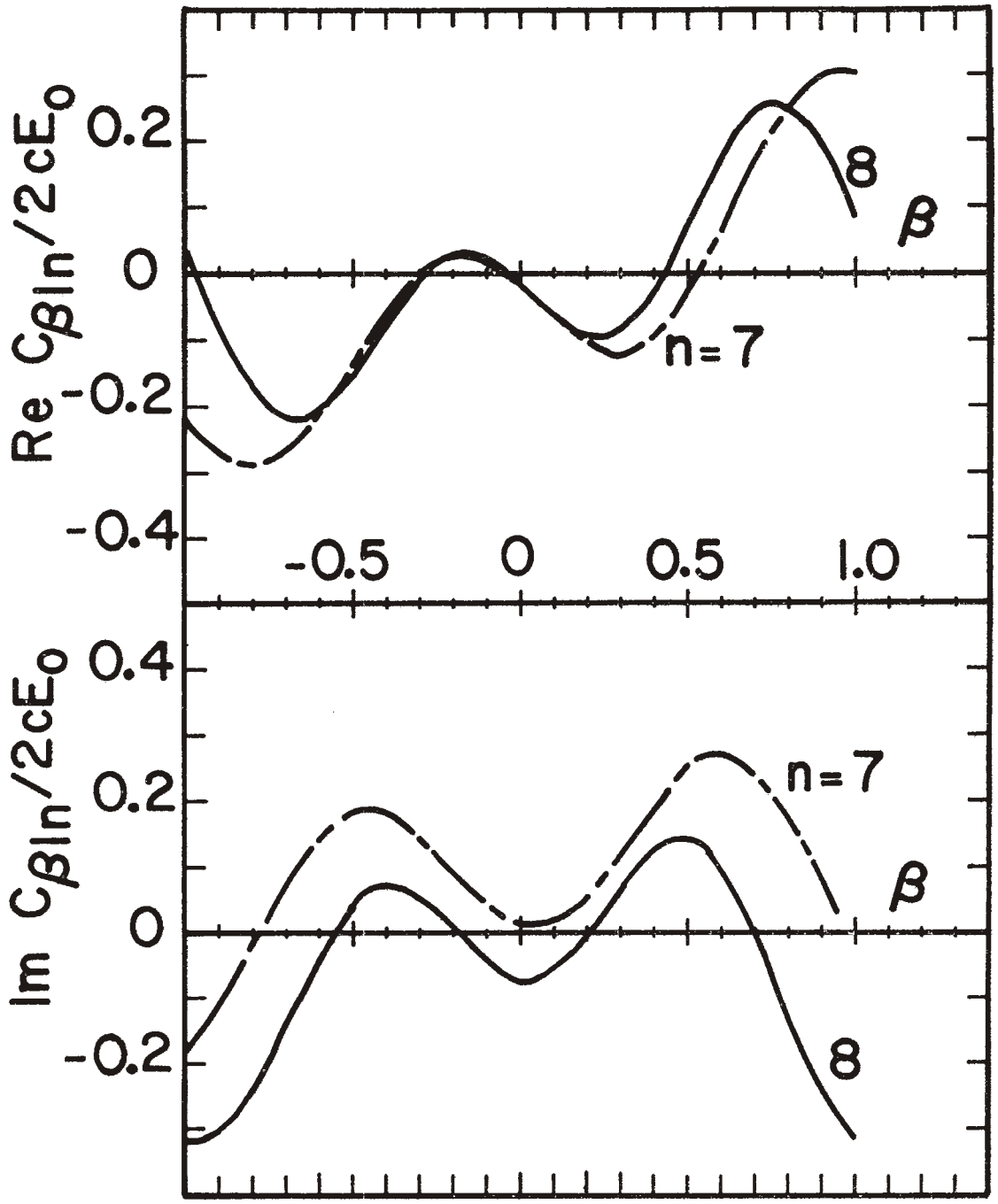

Figure 15b. Coupling coefficient C_β in milliamperes of an L-wire over a ground plane for resonant frequencies S_{17} and S_{18}, r/L = 0.7, d/L = 0.5, $a_1/L = a_2/L = 0.001$.

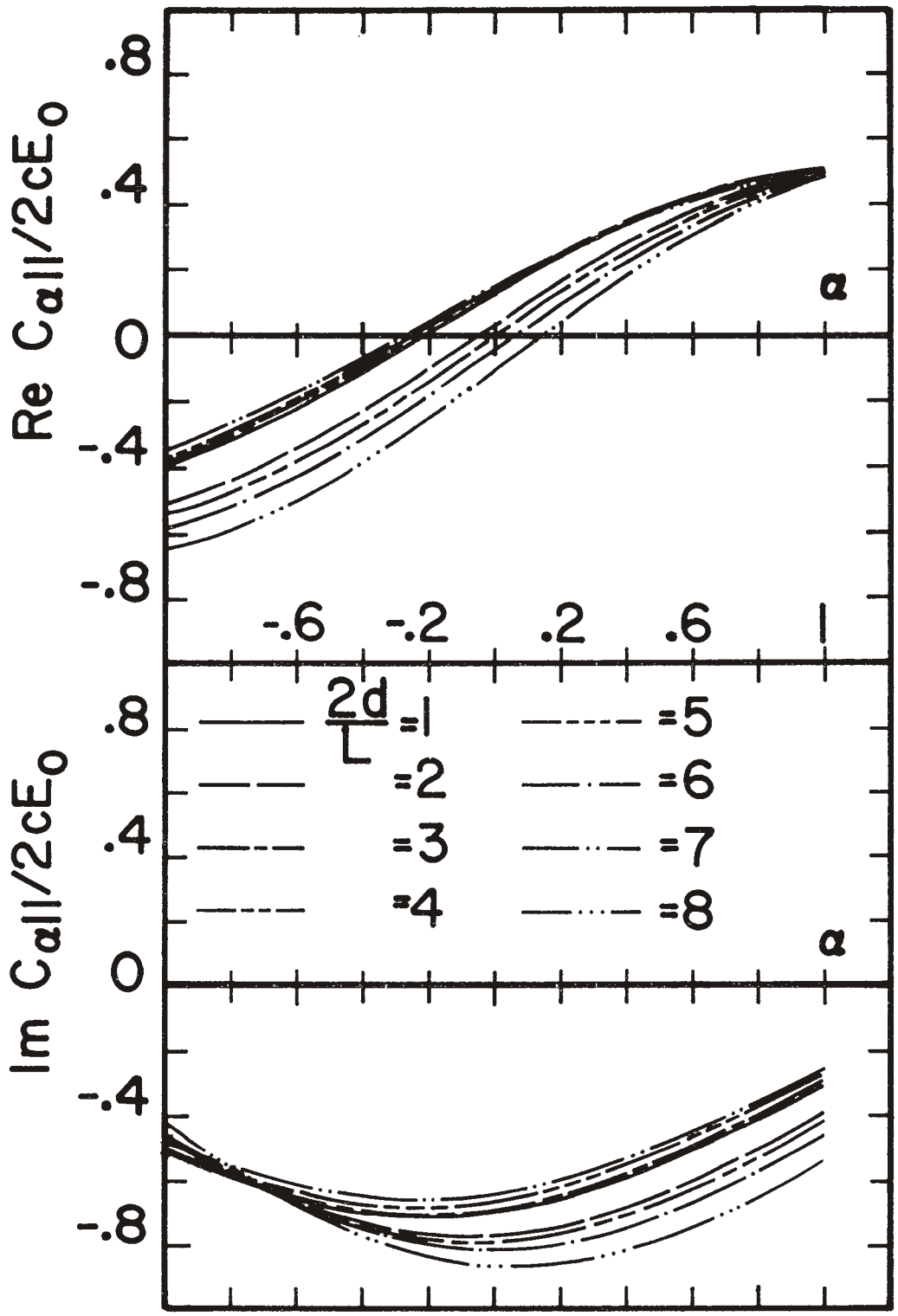

Figure 16a. Coupling coefficient C_α in milliamperes of an L-wire over a ground plane for resonant frequency S_{11} for various distances d, r/L = 0.7, $a_1/L = a_2/L = 0.001$.

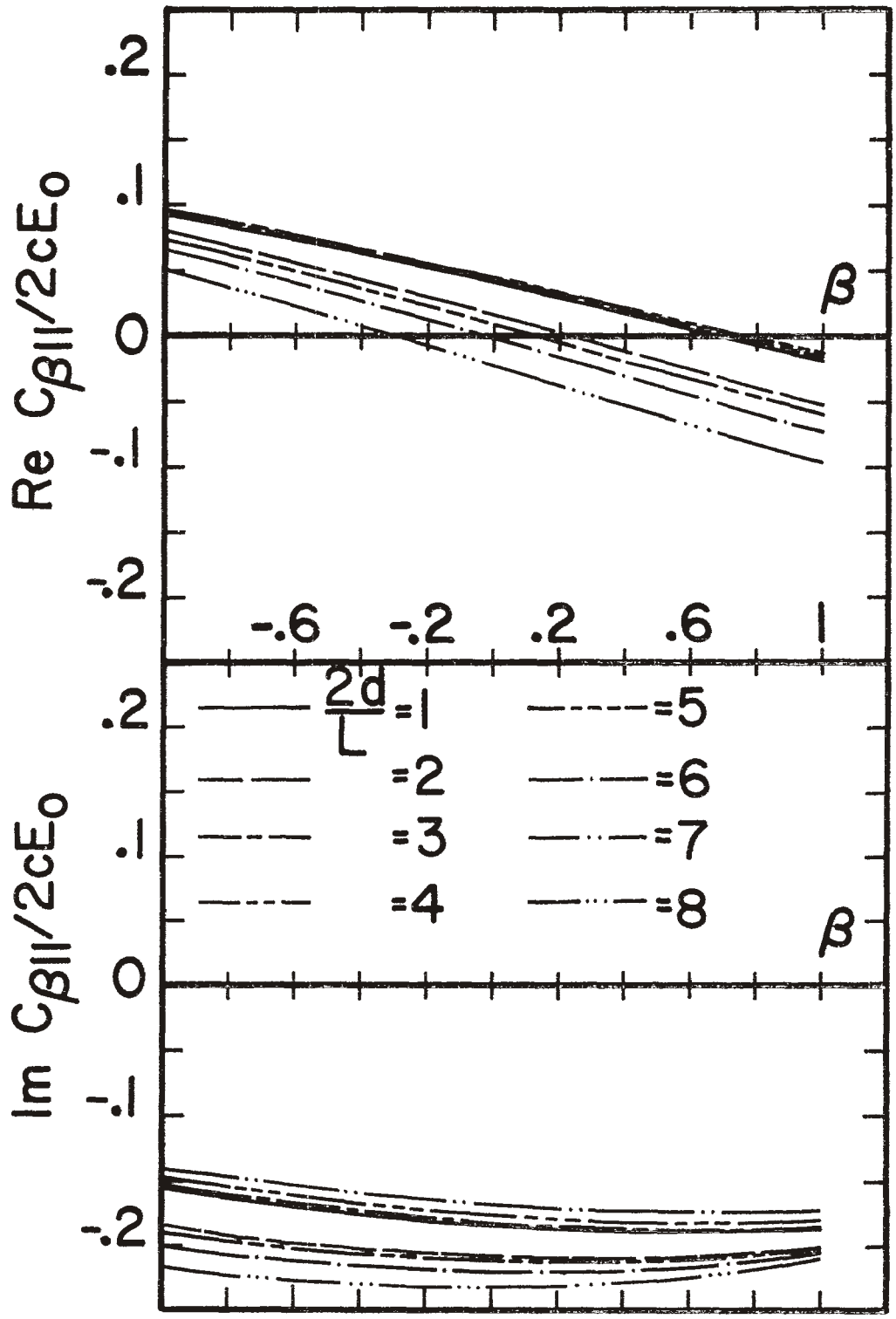

Figure 16b. Coupling coefficient C_β in milliamperes of an L-wire over a ground plane for resonant frequency S_{11} for various distances d, r/L = 0.7, $a_1/L = a_2/L = 0.001$.

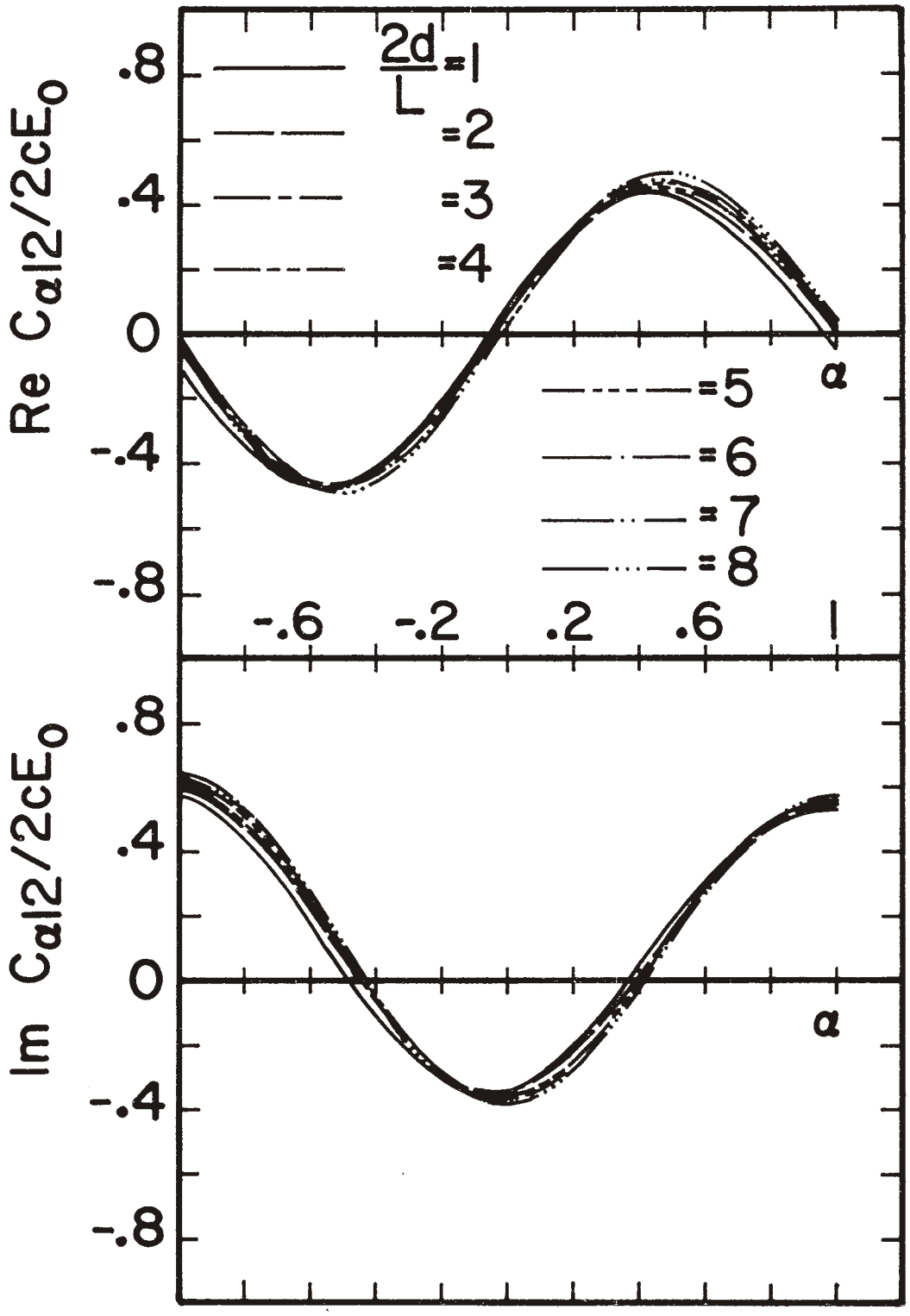

Figure 17a. Coupling coefficient C_α in milliamperes of an L-wire over a ground plane for resonant frequency S_{12} for various distances d, r/L = 0.7, $a_1/L = a_2/L = 0.001$.

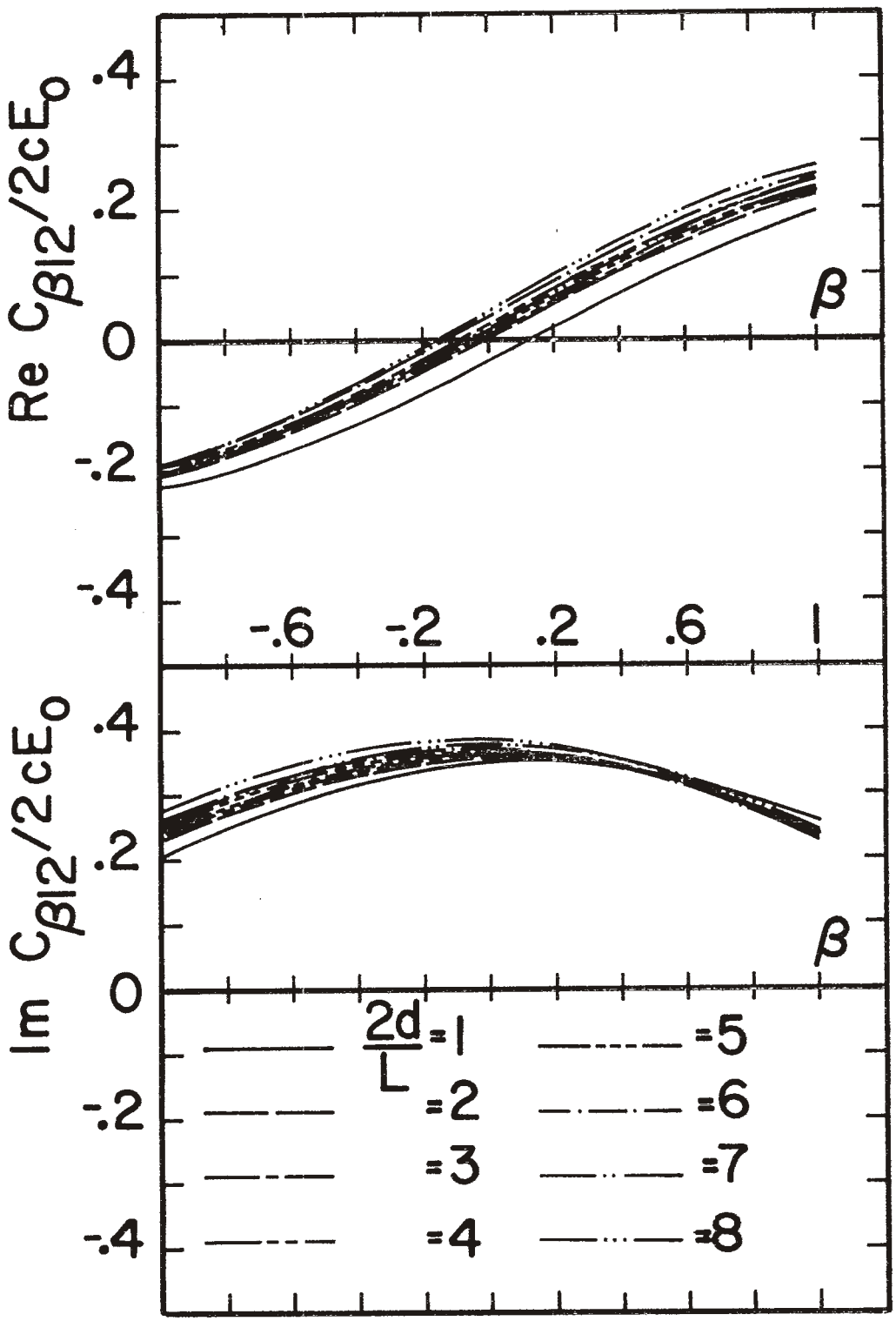

Figure 17b. Coupling coefficient C_β in milliamperes of an L-wire over a ground plane for resonant frequency S_{12} for various distances d, r/L = 0.7, $a_1/L = a_2/L = 0.001$.

and resolving $\overline{V}(s_i)$ into two components

$$C_i = C_{\alpha i} + C_{\beta i} \tag{4.2}$$

where

$$C_{\alpha i} = \beta_i \overline{H}_i^{\dagger} \overline{V}_{\alpha}(s_i) \tag{4.3}$$

and

$$C_{\beta i} = \beta_i \overline{H}_i^{\dagger} \overline{V}_{\beta}(s_i) \tag{4.4}$$

where $\overline{V}_{\alpha}(s_i)$ and $\overline{V}_{\beta}(s)$ are calculated according to (3.4) and (3.5) with the terms

$$E^i_{x\alpha}(s) = E_{0x}\, e^{-\frac{s}{c}\alpha x}$$

$$-1 < \alpha < +1 \tag{4.5}$$

$$E^i_{z\alpha}(s) = 0$$

from which $C_{\alpha i}$ are determined and

$$E^i_{x\beta}(s) = 0$$

$$-1 < \beta < +1 \tag{4.6}$$

$$E^i_{z\beta}(s) = E_{0z}\, e^{-\frac{s}{c}\beta z}$$

from which $C_{\beta i}$ are determined. E_{0x} and E_{0z} are the magnitude scale factors determined by the polarization of the incident electric field

and α and β are the direction cosines with respect to the x and y axes of the ficticious incident field which excites only one of the wire arms.

Neglecting the reflected parts of the field terms due to the ground plane, for E_θ - polarization

$$E_{0x} = E_0 \cos\theta\cos\phi$$

$$E_{0z} = -E_0 \sin\theta$$

$$\alpha = \sin\theta\cos\phi$$

$$\beta = \cos\theta \qquad (4.7)$$

Hence the coupling coefficients presented in Figures 13,14 and 15 show only the effect of the shift in the location of the pole due to the ground plane as compared to the isolated case. The actual coupling coefficients $c_{\alpha i}$ and $c_{\beta i}$ for the L-wire structure over the ground plane can be constructed corresponding to the incident and reflected fields of Equations (3.6) and (3.7) exciting the structure according to

$$c_{\alpha i} = C_{\alpha i}(\alpha)\left[1 - e^{\frac{s_i}{c} 2d\cos\theta}\right] \qquad (4.8)$$

$$c_{\beta i} = C_{\beta i}(-\beta)\, e^{\frac{s_i}{c} 2d\cos\theta} + C_{\beta i}(\beta) \qquad (4.9)$$

The resultant coupling coefficient c_i is obtained by the superposition of the individual coupling coefficients $c_{\alpha i}$ and $c_{\beta i}$.

In terms of coupling coefficients the expression (3.11) may be written as [3]

$$\overline{J}(s) = \sum_i \frac{\overline{J}_i \, c_i}{s - s_i} \tag{4.10}$$

In Figure 18, the frequency domain solution obtained from SEM calculations at three points on the structure is given corresponding to a time harmonic plane wave incident and the results are compared at the junction point by solving the coupled integral equations (2.1) and (2.2) by direct moment method solutions in the frequency domain. In Figures 19 and 20 are given the time domain current and charge distributions as obtained by SEM for E_θ-polarization with a step function plane wave incident and these results are checked at the junction point by direct Fourier inversion of the frequency domain data obtained by solving the coupled integral equations. Figure 21 shows the convergence of the time domain current as the number of poles closest to $j\omega$ - axis is increased.

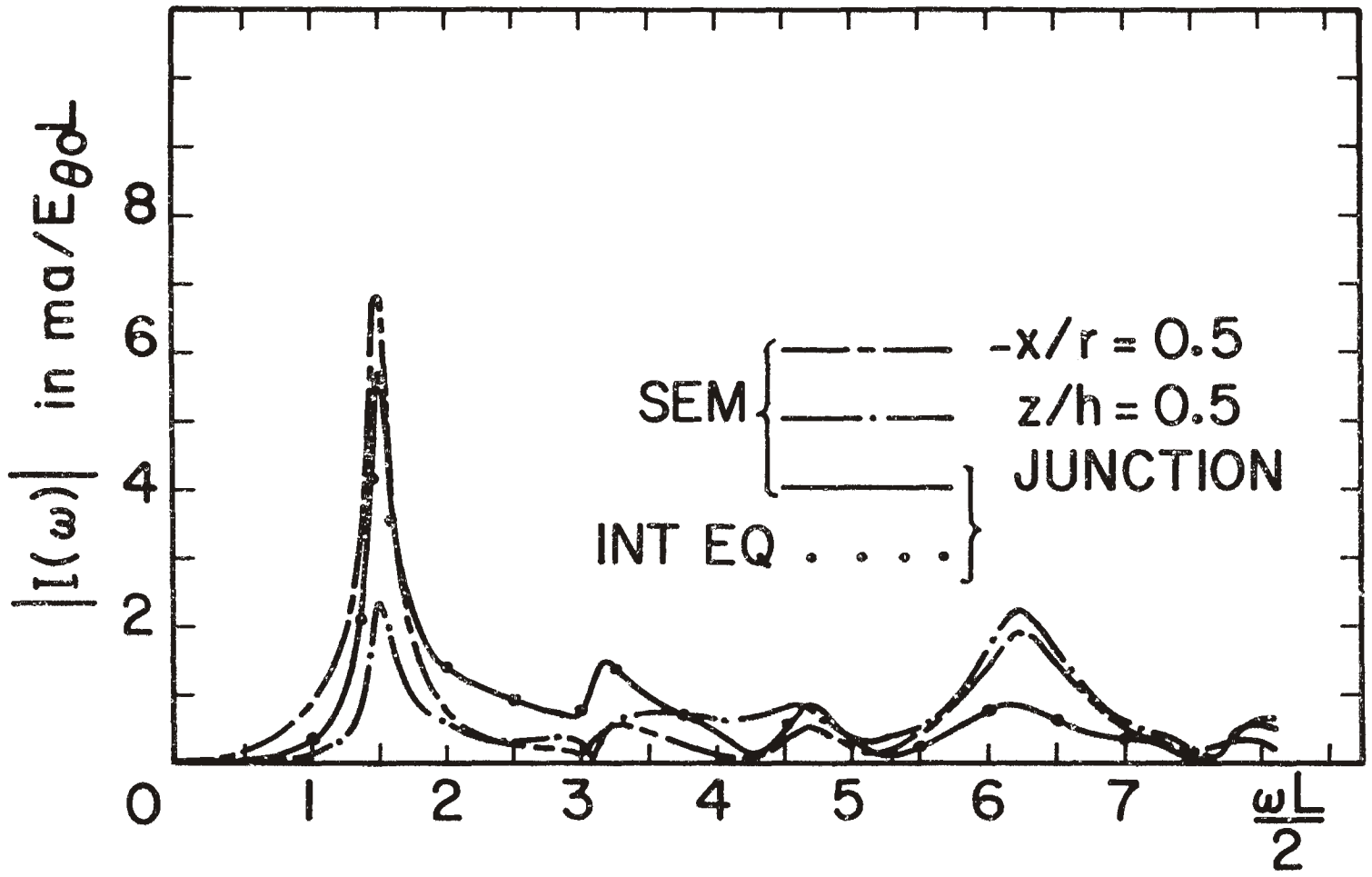

Figure 18. Variation of current on the L-wire as a function of frequency for a plane wave incident, r/L = 0.7, d/L = 0.5, a_1/L = a_2/L = 0.001, θ = 135°, ϕ = 45°, E_θ - polarization.

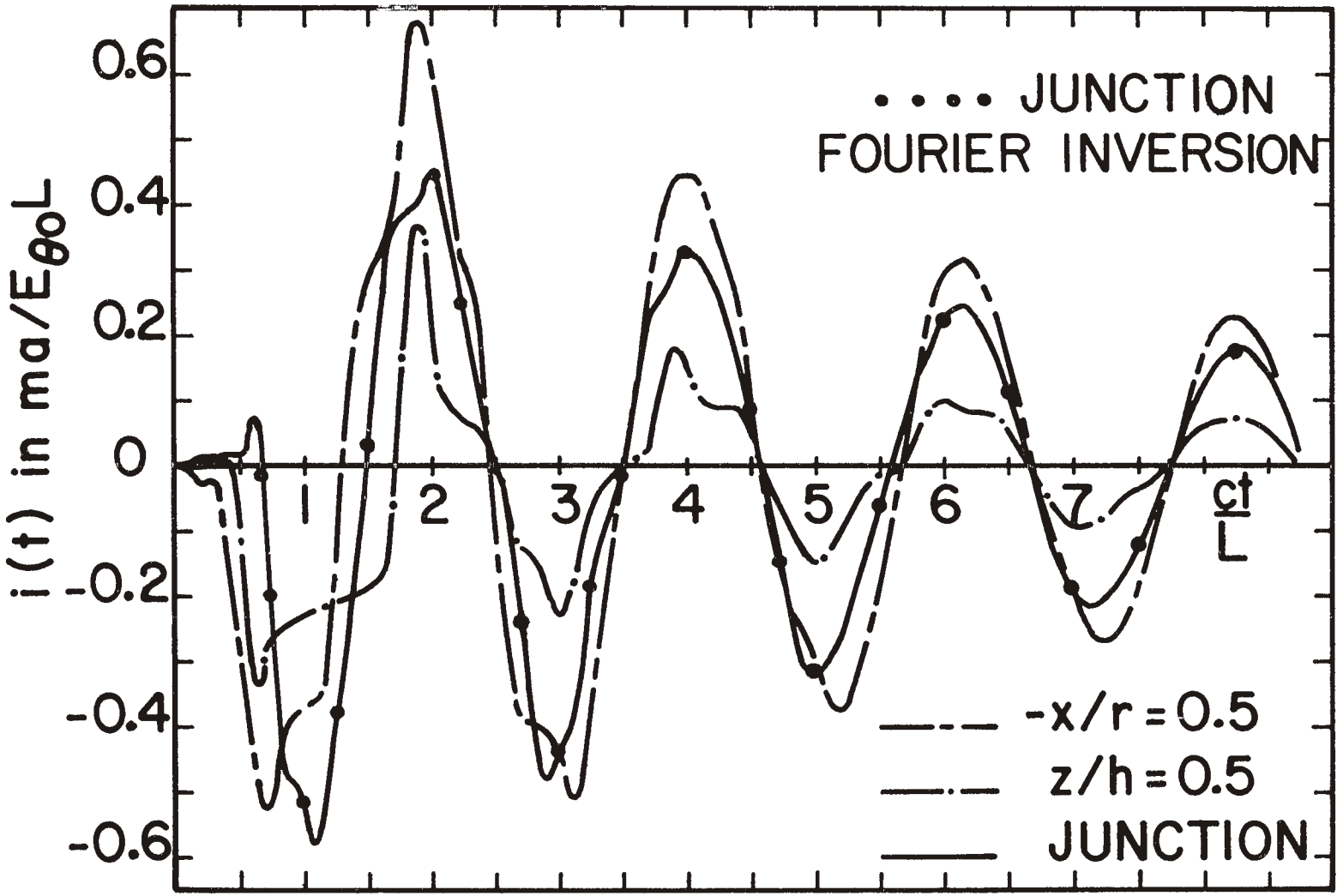

Figure 19. Time domain current, step function plane wave incident, $\theta = 135°$, $\phi = 45°$, E_θ - polarization, t = 0 at x = -r; r/L = 0.7, d/L = 0.5, $a_1/L = a_2/L = 0.001$.

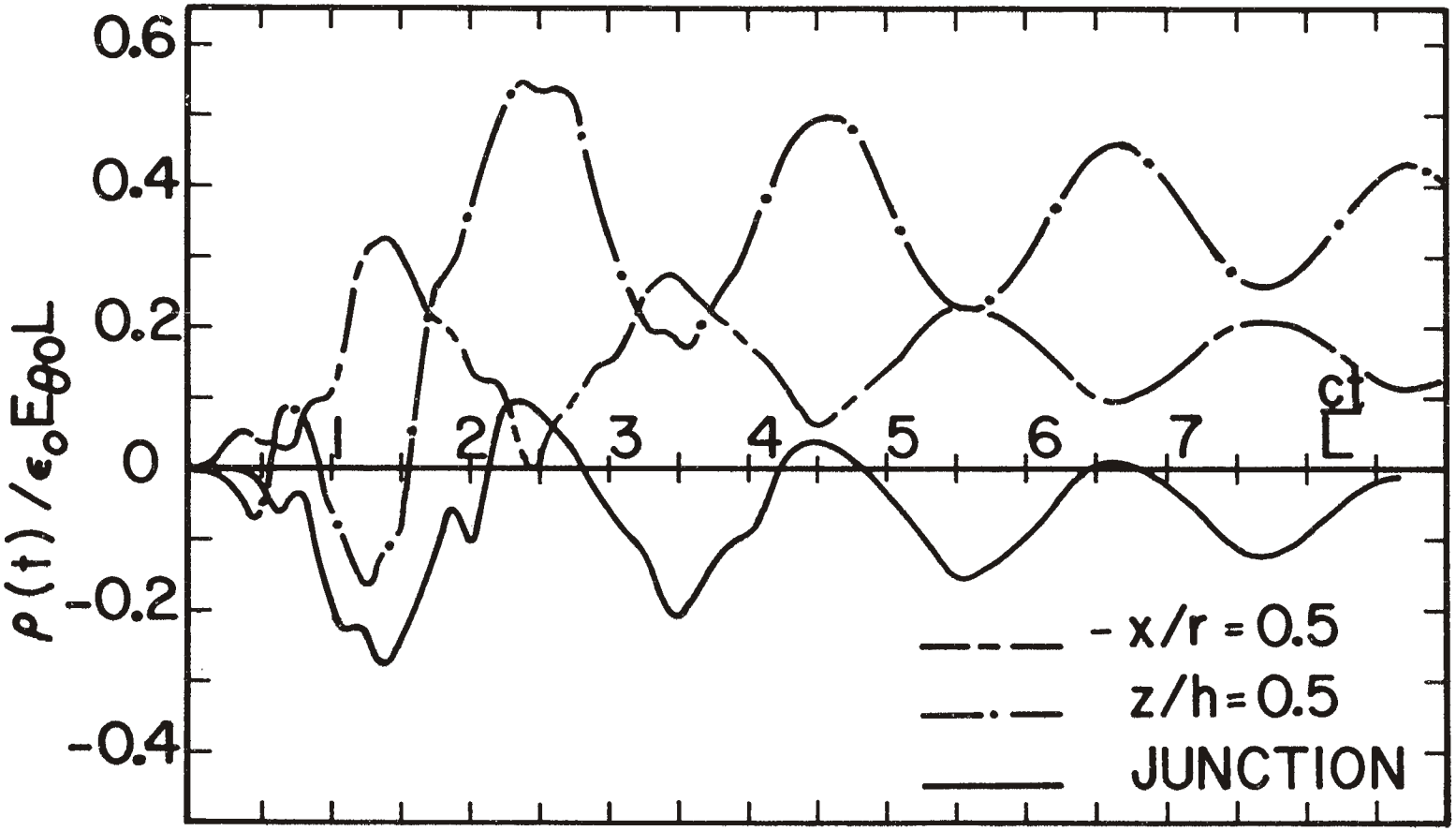

Figure 20. Time domain charge, step function plane wave incident, $\theta = 135°$, $\phi = 45°$, E_θ - polarization, $t = 0$ at $x = -r$; $r/L = 0.7$, $d/L = 0.5$, $a_1/L = a_2/L = 0.001$.

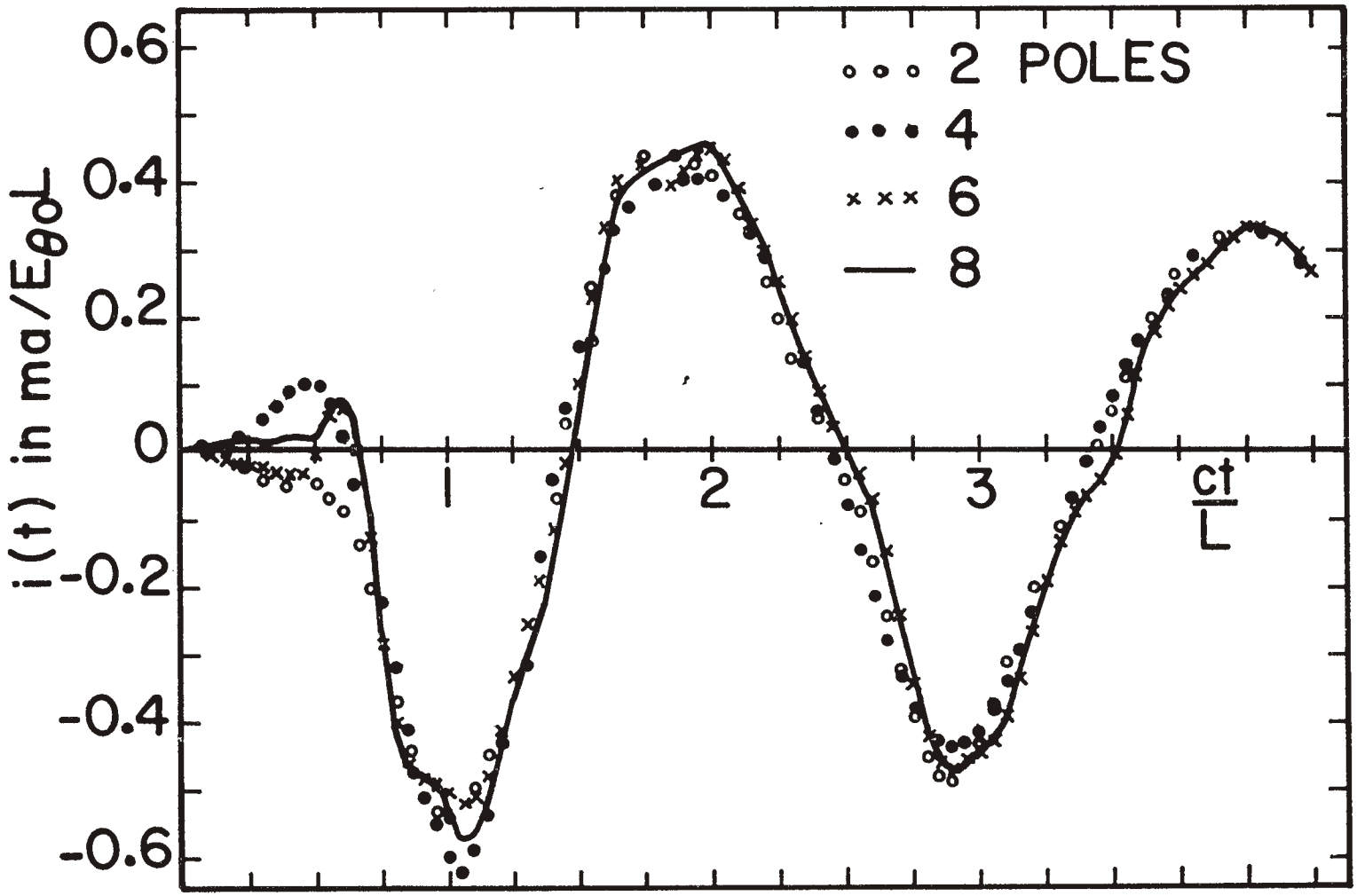

Figure 21. Convergence of time domain current, $\theta = 135°$, $\phi = 45°$, E_θ - polarization, step function plane wave incident, $t = 0$ at $x = -r$; $r/L = 0.7$, $d/L = 0.5$, $a_1/L = a_2/L = 0.001$.

V. CONCLUSIONS

A structure with coupled elements in the form of a L-wire and L-wire over a conducting ground plane can be characterized by SEM. However, in the latter case the results are neither so easily displayed graphically nor so submissive to physical interpretation. This is partially true because of the introduction of another parameter, the distance d above the ground plane, but the primary difficulty is in the complex interactions and trajectories of the poles and the problem of classifying the various pole types which appear. Possibly ground plane effects might be better handled using a multiple scattering approach to account for the interaction of an isolated L-wire and its image.

The pole patterns obtained for the L-wire and the L-wire over the conducting ground plane follow closely those obtained for the circular cylinder and the circular cylinder parallel or perpendicular to the ground plane. The zigzag nature of the location of the poles closest to $j\omega$ - axis is mainly due to the location of the bend on the L-wire structure. It was observed that the bend and the ground plane have minor effects on the distribution of the modal currents. The coupling vector obtained according to Hallen's formulation can no longer be compared to those in the E-field formulation, but the coupling coefficients are the same. The time domain solution is mainly contributed from the poles closest to the $j\omega$ - axis.

REFERENCES

1. Wilton, D.R., and Umashankar, K.R., "Parametric Study of an L-shaped Wire Using the Singularity Expansion Method," EMP Interaction Note 152, November 1973.

2. Harrington, R.F., Field Computation by Moment Methods, MacMillan, New York, 1968.

3. Baum, C.E., "On the Singularity Expansion Method for the Solution of Electromagnetic Interaction Problems," EMP Interaction Note 88, December 1971.

4. Shumpert, T.H., "EMP Interaction with A Thin Cylinder Above a Ground Plane Using the Singularity Expansion Method," Sensor and Simulation Notes, Note 182, June 1973.